Dynamics of complete turbulence suppression in turbidity currents driven by monodisperse suspensions of sediment

Mrugesh Shringarpure, Mariano I. Cantero and S. Balachandar

Journal of Fluid Mechanics / *FirstView* Article / January 2006, pp 1 - 34
DOI: 10.1017/jfm.2012.427, Published online:

J. Fluid Mech., page 1 of 34.
doi:10.1017/jfm.2012.427

Dynamics of complete turbulence suppression in turbidity currents driven by monodisperse suspensions of sediment

Mrugesh Shringarpure[1], Mariano I. Cantero[2,3] and S. Balachandar[1]†

[1] Department of Mechanical and Aerospace Engineering, University of Florida, Gainesville, FL 32611, USA

[2] National Council for Scientific and Technological Research, Bariloche Atomic Center, Bustillo 9500 (CP: 8400), Río Negro, San Carlos de Bariloche, Argentina

[3] Institute Balseiro, National Commission of Atomic Energy, National University of Cuyo, San Carlos de Bariloche, Av. Bustillo 9500, Bariloche - Río Negro (8400), Río Negro, Argentina

(Received 4 February 2012; revised 22 August 2012; accepted 27 August 2012)

Turbidity currents derive their motion from the excess density imposed by suspended sediments. The settling tendency of sediments is countered by flow turbulence, which expends energy to keep them in suspension. This interaction leads to downward increasing concentration of suspended sediments (stable stratification) in the flow. Thus in a turbidity current sediments play the dual role of sustaining turbulence by driving the flow and damping turbulence due to stable stratification. By means of direct numerical simulations, it has been shown previously that stratification above a threshold can substantially reduce turbulence and possibly extinguish it. This study expands the simplified model by Cantero *et al.* (*J. Geophys. Res.*, vol. 114, 2009*a*, C03008), and puts forth a proposition that explains the mechanism of complete turbulence suppression due to suspended sediments. In our simulations it is observed that suspensions of larger sediments lead to stronger stratification and, above a threshold size, induce an abrupt transition in the flow to complete turbulence suppression. It has been widely accepted that hairpin and quasi-streamwise vortices are key to sustaining turbulence in wall-bounded flows, and that only vortices of sufficiently strong intensity can spawn the next generation of vortices. This auto-generation mechanism keeps the flow populated with hairpin and quasi-streamwise vortical structures and thus sustains turbulence. From statistical analysis of Reynolds stress events and visualization of flow structures, it is observed that settling sediments damp the Reynolds stress events (Q2 events), which means a reduction in both the strength and spatial distribution of vortical structures. Beyond the threshold sediment size, the existing vortical structures in the flow are damped to an extent where they lose their ability to regenerate the subsequent generation of turbulent vortical structures, which ultimately leads to complete turbulence suppression.

Key words: geophysical and geological flows, turbidity currents, turbulence suppression

† Email address for correspondence: bala1s@ufl.edu

1. Introduction

Horizontal density differences in a fluid under the action of a gravitational field result in flows known as gravity currents (Hopfinger 1983; Allen 2001). Turbidity currents are special cases of gravity currents where suspended sediments are responsible for the density difference. Turbidity currents are predominantly ocean currents flowing along the ocean floor. They can be triggered by various mechanisms, but essentially a turbidity current involves sediments flowing down the sloping ocean floor dragging the surrounding water with it. The resulting flow is typically turbulent, which in turn keeps the sediments in suspension to drive the flow. Turbidity currents are known to reach speeds of the order of 5 m s^{-1} in submarine canyons (Krause *et al.* 1970) and travel hundreds of kilometres (Pirmez & Imran 2003). This ability to reach high speeds and travel long distances makes turbidity currents an important sediment transport mechanism in the submarine world (Kneller & Buckee 2000).

Suspended sediments play a crucial role in both sustaining and killing turbidity currents. The increased density due to the suspended sediments drives the flow, and the generated turbulence provides the energy required to keep the sediments in suspension. The distribution of suspended sediments in a turbidity current is governed by balance between downward flux of sediments due to settling and upward flux of sediments due to turbulent mixing. This exchange leads to a stable stratification of sediments in the flow. This stratification suppresses turbulence by limiting the exchange of mass and momentum in the bed-normal direction, and in extreme cases can lead to complete shutdown of turbulence. In such extreme cases, absence of turbulence leads to heavy deposition of sediments, which results in complete cessation of the flow (Talling *et al.* 2007; Cantero *et al.* 2012*a*). This dual role of sediments makes the flow interesting and complex to analyse. In this work we dissect these two roles using direct numerical simulation (DNS) and attempt to explain how suspended sediments affect flow turbulence.

In an actual turbidity current there are sediments of various sizes (Parker 2008) and the flow itself is highly turbulent with a large Reynolds number of $O(10^6)$ or more. Sufficiently large sediments do not get suspended into the flow, but are transported along the bed as bedload through rolling and occasional saltation. On the other hand, washload sediments are so fine that they effectively do not settle, and remain well mixed in the flow. The effect of washload is to make the fluid heavier than its surroundings. This work focuses on the intermediate size of sediments, which settle towards the bed and can be re-entrained into suspension by turbulence. The particular limit where the rate of deposition is exactly balanced by the rate of resuspension is considered, and thus the total amount of suspended sediments is conserved in the flow. The current in which there is zero net flux of sediments to the ocean bed is said to be in bypass or auto-suspension mode. In other words, the driving potential of such a current is always conserved. This regime of sediment transport is the limit between the depositional mode, for which the net amount of sediments decay over time or distance of spreading leading to ultimate cession of the current, and the resuspension mode, for which the net amount of sediments increases along with the intensity of the current (Parker 1982; Parker, Fukushima & Pantin 1986).

Direct numerical simulation of a field-scale turbidity current is not possible even with the current state-of-the-art high-performance computers. In order to gain fundamental understanding of the effects of suspended sediments on turbulence, simulations must be restricted to low and moderate Reynolds number turbidity currents. The understanding gained from such simulations can then be extrapolated and used in various models of field-scale turbidity currents. Recent investigations of turbulent

turbidity currents using the 'turbidity current with a roof' (TCR) model (Cantero *et al.* 2009*a*; Cantero, Balachandar & Parker 2009*b*) demonstrate that turbulence can be completely damped when the settling velocity of sediments exceed a certain threshold value. This study extends the work by Cantero *et al.* (2009*a*,*b*) in a significant way to obtain a comprehensive understanding of the mechanism of total turbulence suppression. The earlier theoretical model (TCR) employed an artificial rigid top boundary, which somewhat complicated its direct applicability to actual turbidity currents. As a result, even when stratification suppressed turbulence close to the bottom boundary, turbulence continued to generate near the rigid top boundary and diffused downward to the bottom boundary, thus influencing turbulence suppression by stratification. This feature affected identification of the suppression mechanism and prevented clear interpretation of the results. Here a model of equilibrium turbidity currents that uses a stress-free top boundary is implemented, which limits turbulence generation to only the bottom boundary. The present approach allows complete suppression of turbulence over the entire layer of fluid. However, as in the TCR model, the slow streamwise development of the current is ignored by not allowing entrainment of ambient fluid.

The model presented in this work preserves the essential features of turbidity currents, i.e. the flow is entirely driven by the suspended sediments and the settling of sediments self-stratifies the flow. These features are representative of an actual turbidity current in the bypass mode. The present model has been used to separate the driving and the stratification effects of the suspended sediments by individually turning these effects on and off. The most intriguing aspect of the results is the abrupt nature of total turbulence suppression with increase in the settling velocity of sediments (a proxy for the size of sediments). More precisely, below a threshold value of settling velocity the turbidity current remains vigorously turbulent, and the level of turbulence is only moderately influenced by the suspended sediments. However, once the threshold value is crossed, an abrupt change in behaviour occurs and turbulence is totally extinguished. This abrupt transition is akin to the onset of instability in a laminar flow, but the key difference is that the nature of reverse-transition to laminar conditions is inherently nonlinear. This work further explores this transition both from a statistical point of view and also from a mechanistic point of view in terms of how the auto-generation of turbulent vortical structures is completely disrupted above the threshold.

The mathematical model of turbidity currents employed in this study serves the purpose of developing fundamental understanding of interaction of suspended sediments and turbulence. Existence of a critical settling velocity for a given Re_τ and channel slope θ has practical implications. This observation means that only a certain size of sediments can be kept in suspension in a flow of given intensity. The knowledge we gain brings us closer to understanding the transition of turbidity currents from being net erosional (self-accelerating) to net depositional. The validation of this simple, yet effective mathematical model is difficult, as laboratory experiments cannot recreate such conditions and the field observations are too complex to be exactly relevant. However, some indirect indications of turbulence suppression exist. Experiments by Sequeiros *et al.* (2009) show transition from net erosional to net depositional flow. In such a transition the net depositional flow will eventually lead to complete shutdown of turbulence and the flow. However, in the laboratory this eventual state cannot be observed owing to the size constrains of the flume. Talling *et al.* (2007) reported field observations that sudden turbulence suppression can occur,

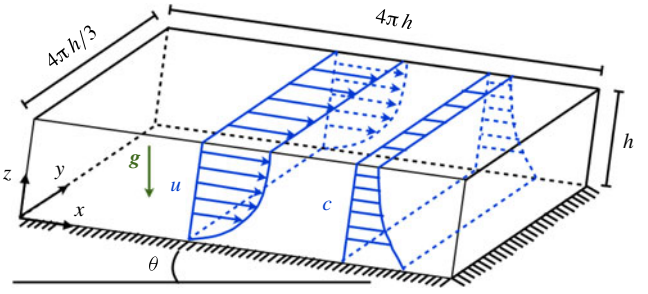

FIGURE 1. (Colour online) Schematic representation of the model of a turbidity current. The model preserves the most essential features of turbidity currents, i.e. the flow is entirely driven by the suspended sediments and the settling of sediments self-stratifies the flow.

leading to abrupt loss of carrying capacity of the flow, in turn leading to heavy sedimentation.

2. Problem formulation

The turbidity current is modelled as an inclined channel with a slope of θ with respect to the horizontal. The flow in the channel is driven by a monodisperse suspension of sediments which drag the fluid in the streamwise direction and also settle down, stratifying the flow (see figure 1). The suspension is assumed to be dilute so that collision between sediment particles and rheology effects can be neglected, settling velocity is independent of concentration, and Boussinesq approximation can be employed. Under these circumstances the flow is governed by the following equations:

$$\frac{\partial \boldsymbol{u}}{\partial t} + \boldsymbol{u}\cdot\boldsymbol{\nabla}\boldsymbol{u} = -\frac{1}{\rho_w}\boldsymbol{\nabla}p + \nu\nabla^2\boldsymbol{u} + \frac{\rho-\rho_w}{\rho_w}\boldsymbol{g}, \tag{2.1}$$

$$\boldsymbol{\nabla}\cdot\boldsymbol{u} = 0, \tag{2.2}$$

$$\frac{\partial c}{\partial t} + (\boldsymbol{u}+\boldsymbol{V})\cdot\boldsymbol{\nabla}c = \mathscr{D}\nabla^2 c, \tag{2.3}$$

where $\boldsymbol{u} = \{u, v, w\}$ is the velocity vector, p is the pressure, ρ_w is the density of water, ν is the kinematic viscosity of water, c is the volumetric concentration of sediments, $\rho = \rho_w(1 + Rc)$ is the density of the mixture with $R = (\rho_s - \rho_w)/\rho_w$ and ρ_s the density of the sediments, $\boldsymbol{g} = \{g_x, 0, -g_z\}$ is the acceleration due to gravity with g_x and g_z the components along the streamwise and bed-normal directions of the channel, $\boldsymbol{V} = \{V_x, 0, -V_z\}$ is the terminal settling velocity of an isolated sediment particle in a quiescent ambient, and $\mathscr{D}$ is the diffusivity of the sediments. By using these equations it is assumed that the inertial effects of the sediments are of second order compared to settling effects (Ferry & Balachandar 2001; Cantero, Balachandar & García 2008*a*; Cantero, García & Balachandar 2008*c*).

Sediment particles are assumed to be non-cohesive and large enough that their Brownian motion can be ignored. It is now well established that even such large particles effectively diffuse due to long-range hydrodynamic interactions mediated by particle number density fluctuations (Segre *et al.* 2001; Mucha & Brenner 2003). Thus $\mathscr{D}$ is taken to be the effective constant diffusivity of the sediments. The diffusive term in (2.3) also provides a mechanism to resuspend sediments from the bed (Garcia & Parker 1993).

The channel is assumed to be periodic in the streamwise and spanwise directions. The height of the simulation domain is h. The length of the simulation domain (streamwise direction) is $L_x = 4\pi h$ and the width (spanwise direction) is $L_y = 4\pi h/3$. Along the streamwise and spanwise directions periodic boundary conditions are imposed for all variables. The top boundary of the channel is smooth with a no-stress boundary condition, while the bottom boundary represents the bed where a no-slip condition is imposed. The top and bottom boundary conditions for concentration state that settling exactly balances resuspension. Thus, for the top and bottom boundaries the imposed boundary conditions are

$$\boldsymbol{u} = 0 \quad \text{at } z = 0, \tag{2.4}$$

$$\frac{\partial u}{\partial z} = 0, \quad \frac{\partial v}{\partial z} = 0 \quad \text{and} \quad w = 0 \quad \text{at } z = h, \tag{2.5}$$

$$-cV_z = \mathscr{D}\frac{\partial c}{\partial z} \quad \text{at } z = 0 \quad \text{and} \quad z = h. \tag{2.6}$$

An important consequence of assuming (2.6) is that the net volume concentration of sediments within the domain is conserved. This allows for the statistically stationary state of the turbulent flow.

2.1. *Mean flow equations*

The problem defined in § 2 has a fully developed statistically stationary state. The mean flow equations obtained by averaging the momentum and concentration equations over turbulence read

$$\nu\frac{\mathrm{d}^2\bar{u}}{\mathrm{d}z^2} - \frac{\mathrm{d}}{\mathrm{d}z}(\overline{u'w'}) + R\bar{c}g_x = 0, \tag{2.7}$$

$$\frac{1}{\rho_w}\frac{\mathrm{d}\bar{p}}{\mathrm{d}z} + \frac{\mathrm{d}}{\mathrm{d}z}(\overline{w'^2}) + R\bar{c}g_z = 0, \tag{2.8}$$

and

$$\mathscr{D}\frac{\mathrm{d}^2\bar{c}}{\mathrm{d}z^2} + V_z\frac{\mathrm{d}\bar{c}}{\mathrm{d}z} - \frac{\mathrm{d}}{\mathrm{d}z}(\overline{c'w'}) = 0. \tag{2.9}$$

Here, the mean variables are represented by an overbar $(\bar{\cdot})$ and the fluctuations from the mean are represented by a prime $(\cdot')$. Averaging is performed over time and over the two homogeneous directions x and y. Since there is no gravitational acceleration along the spanwise direction (y), the mean flow is assumed two-dimensional with $\bar{v} = 0$. Furthermore, owing to the incompressibility of the fluid and to the no-penetration condition at the top and bottom boundaries, $\bar{w} = 0$.

Observe that pressure appears only in (2.8), from which

$$p^* = \bar{p} + \rho_w\overline{w'^2} + \rho_w R g_z\int_0^z \bar{c}(\eta)\,\mathrm{d}\eta, \tag{2.10}$$

where p^* is the mean dynamic pressure that remains after subtracting the hydrostatic pressure due to suspended sediments, and its only role is to ensure the incompressibility condition.

From (2.7) the bottom shear stress τ_b can be expressed as

$$\frac{\tau_b}{\rho_w} = Rg_x\int_0^h \bar{c}(z)\,\mathrm{d}z, \tag{2.11}$$

since the stress at the top boundary is zero and the Reynolds stress ($\overline{u'w'}$) is zero at the top and bottom boundaries. Based on (2.11), a velocity scale is defined as

$$u_*^2 = \frac{\tau_b}{\rho_w} = Rg_x\bar{c}^{(v)}h, \tag{2.12}$$

where

$$\bar{c}^{(v)} = \frac{1}{h}\int_0^h \bar{c}(z)\,\mathrm{d}z \tag{2.13}$$

is the volume-averaged sediment concentration.

It is apparent that for $V = |\boldsymbol{V}| = 0$ the sediment concentration will remain well mixed without any vertical gradient, i.e. $\mathrm{d}\bar{c}/\mathrm{d}z = 0$. In this limit the problem reduces to a channel flow driven by a uniform body force given by $\rho_w R g_x \bar{c}^{(v)}$.

Following the work by Geyer (1993), turbulent sediment fluxes can be approximated as

$$-\overline{w'c'} = \mathscr{D}_t\frac{\mathrm{d}\bar{c}}{\mathrm{d}z}, \tag{2.14}$$

where $\mathscr{D}_t = \kappa u_* z(1 - z/H)$ is the turbulent diffusivity and κ is the constant in the velocity log law ($u^+ = (1/\kappa)\log(z^+) + B$). Equation (2.9) can be integrated to the Rouse profile

$$\frac{\bar{c}}{\bar{c}_b} = \left[\frac{(H-z)/z}{(H-b)/b}\right]^{Ro}, \tag{2.15}$$

where Ro is the Rouse number given by $Ro = V_z/\kappa u_*$, $b = 0.01H$ and $\bar{c}_b$ is the value of concentration at $z = b$.

2.2. *Dimensionless equations*

The following scales are employed to define dimensionless variables: u_* for velocity, h for length, h/u_* for time, $\bar{c}^{(v)}$ for concentration of sediments, and $\rho_w u_*^2$ for pressure. The dimensionless governing equations are

$$\frac{\partial\tilde{\boldsymbol{u}}}{\partial\tilde{t}} + \tilde{\boldsymbol{u}}\cdot\tilde{\boldsymbol{\nabla}}\tilde{\boldsymbol{u}} = -\tilde{\boldsymbol{\nabla}}\tilde{p} + \frac{1}{Re_\tau}\tilde{\nabla}^2\tilde{\boldsymbol{u}} + \tilde{c}\,\boldsymbol{e}_g, \tag{2.16}$$

$$\tilde{\boldsymbol{\nabla}}\cdot\tilde{\boldsymbol{u}} = 0, \tag{2.17}$$

$$\frac{\partial\tilde{c}}{\partial\tilde{t}} + (\tilde{u} + \tilde{V})\cdot\tilde{\boldsymbol{\nabla}}\tilde{c} = \frac{1}{Re_\tau Sc}\tilde{\nabla}^2\tilde{c}, \tag{2.18}$$

where $\boldsymbol{e}_g = \{1, 0, -1/\tan\theta\}$ and $\tan\theta = g_x/g_z$. Dimensionless variables are represented by $(\tilde{\cdot})$. The dimensionless numbers in (2.16)–(2.18) are the Reynolds number (Re_τ) and the Schmidt number (Sc), which are defined as

$$Re_\tau = \frac{u_* h}{\nu} \quad \text{and} \quad Sc = \frac{\nu}{\mathscr{D}}. \tag{2.19}$$

The other two parameters involved in the model are the non-dimensional sediment settling velocity $|\tilde{\boldsymbol{V}}| = \tilde{V}$ and the slope of the channel $\tan\theta$. Note that the above mathematical model, with (2.6) as concentration boundary condition, considers the sedimentation and resuspension fluxes to balance each other locally and instantaneously. This indicates that sediments that settle on the bed are instantly

Case	$\tilde{V}$	$\tilde{u_b}$	Re_b	$\tilde{\bar{c}}_b$	$\tilde{\bar{c}}_t$	κ	B
0	0.0	15.52	2794	1.00	1.00	0.410	5.50
1	0.01	16.13	2903	1.22	0.82	0.348	4.40
2	0.02	17.09	3076	1.55	0.58	0.272	1.82
3	0.025	18.06	3251	1.83	0.44	0.241	0.80
4	0.0255	18.15	3266	1.88	0.43	0.238	0.80
5	0.026	18.33	3300	1.93	0.42	0.237	0.80
6	0.0265	27.32	4900	4.78	0.043	—	—
S1	0.025	15.62	2811	1.58	0.67	0.410	5.8
S2	0.1	15.63	2813	7.63	0.13	0.480	7.6

TABLE 1. List of simulations: $\tilde{V}$ is the dimensionless settling velocity of the sediments, $\tilde{u}_b$ is the bulk velocity of the flow, Re_b is the Reynolds number based on bulk velocity, $\tilde{\bar{c}}_b$ and $\tilde{\bar{c}}_t$ are the dimensionless mean volume concentration of sediments at the bed and the top boundary, and κ and B are the best fit constants for the velocity log law ($u^+ = 1/\kappa \log(z^+) + B$). Values of κ and B for case 6 are not shown as there is complete turbulence suppression and the log-law velocity profile is absent.

resuspended back into the flow. This strong assumption implies that the flow is in the bypass mode for all the cases to be simulated, even as we vary the settling velocity. Note that in real turbidity currents, in order to strictly remain in the bypass mode, an increase in settling velocity must be accompanied by a corresponding increase in the driving force.

Typically the inclination of the continental slope on the ocean floor ranges from 1° to 10° (Pinet 2006), hence the slope of the channel in all the simulations is fixed at $\theta = 5°$ and $1/\tan\theta = 11.43$. For the case of a field turbidity current of height $h = 20$ m running on a slope of $\theta = 5°$ with a mean volume concentration $\bar{c}^{(v)} = 0.005$ of sand particles in water ($R = 1.65$ and $\nu = 10^{-6}$ m^2 s^{-1}), the definition in (2.12) gives $u_* = 0.38$ m s^{-1}. The corresponding V for sediment diameters 70 and 120 μm are $V = 0.004$ m s^{-1} and $V = 0.01$ m s^{-1} (Parker 2008), with corresponding $\tilde{V}_z = 1 \times 10^{-2}$ and $\tilde{V}_z = 2.6 \times 10^{-2}$, respectively. The corresponding Reynolds number ($Re_\tau = 7.5 \times 10^6$) is too large and cannot be studied via DNS. The present simulations employ $Re_\tau = 180$, which results in a mature turbulent flow. Following Segre *et al.* (2001) and Mucha & Brenner (2003), a rough approximation for sediment diffusivity is $\mathscr{D} \approx 10aV$, where a is the radius of the sediment particles. Thus, for the above example $\mathscr{D} \approx 1.5$–6.1×10^{-6} m^2 s^{-1}. It should be noted that $\mathscr{D}$ will depend on the local concentration, concentration gradient and shear stress, but we suppress such dependences in our present model. Based on the findings of Necker *et al.* (2005) and Cantero *et al.* (2008*b*) that the simulation results of turbidity currents are insensitive to the precise values of Sc as long as it is $O(1)$, the present simulations employ $Sc = 1$. Table 1 shows the list of cases studied.

The body force term in (2.16) can be redefined as

$$\tilde{c}\,\boldsymbol{e}_g = (\tilde{c}^{av} + \tilde{c}^*)\left(\hat{\boldsymbol{e}}_x - \frac{\hat{\boldsymbol{e}}_z}{\tan\theta}\right), \tag{2.20}$$

where $\tilde{c}^{av}$ is the instantaneous concentration averaged over planes parallel to the bed, $\tilde{c}^*$ is the corresponding fluctuation from the average concentration field and $\hat{\boldsymbol{e}}_x$ and $\hat{\boldsymbol{e}}_z$ are unit vectors in the $\tilde{x}$ and $\tilde{y}$ directions respectively. The terms in the above equation

can be grouped as follows:

$$\tilde{c}\,\boldsymbol{e}_g = (\tilde{c}^{av} + \tilde{c}^{*})\hat{\boldsymbol{e}}_x - \frac{\tilde{c}^{av}}{\tan\theta}\hat{\boldsymbol{e}}_z - \frac{\tilde{c}^{*}}{\tan\theta}\hat{\boldsymbol{e}}_z. \tag{2.21}$$

The second term on the right in the above equation can be combined with the pressure gradient term in the governing equation (2.16), and the rearranged pressure field is given by

$$\hat{p} = \tilde{p} - \frac{1}{\tan\theta}\int_0^{\tilde{z}} \tilde{c}^{av}(\eta)\,\mathrm{d}\eta. \tag{2.22}$$

The present numerical simulations set the bed-normal pressure gradient to be zero at the top and bottom boundaries, and the above definition of pressure is essential to avoid formation of a spurious pressure boundary layer in the domain.

The bulk velocity of the flow is defined as follows:

$$\tilde{u}_b = \int_0^1 \overline{\tilde{u}}(\tilde{z})\,\mathrm{d}\tilde{z}. \tag{2.23}$$

The bulk Reynolds number can be defined as $Re_b = u_b h/\nu$. The corresponding values of bulk velocity $\tilde{u}_b$ and bulk Reynolds number Re_b for all the cases are listed in table 1. For $Re_\tau = 180$ the bulk Reynolds number is of the order of 3500 and the unstratified flow is turbulent.

The dimensionless governing equations (2.16)–(2.18) are solved using a dealiased pseudo-spectral code (Canuto *et al.* 1988). Fourier expansions are employed in the directions tangential to the bed (x–y), while a Chebyshev expansion is used in the direction normal to the bed (z). A splitting method is used to solve the momentum equation and the incompressibility condition. A low-storage mixed third-order Runge–Kutta and Crank–Nicolson scheme is used for temporal discretization of advection and diffusion terms. This scheme is carried out in three stages with pressure correction at the end of each stage. Details on the implementation of this scheme can be found in the work by Cortese & Balachandar (1995). The grid resolution is $(N_x, N_y, N_z) = (96, 96, 97)$.

3. Laminar solution

The laminar solution of the governing equations is of academic interest only. Note that the laminar flow will not be realized since it is not possible for the finite-sized sediments to stay in suspension without the presence of turbulent mixing and turbulent sediment resuspension from the bed. The laminar solution is, however, useful in establishing total suppression of turbulence.

The laminar flow is assumed to be one-dimensional, steady and uniform. This means that $\tilde{v} = 0$, $\tilde{w} = 0$, $\partial/\partial\tilde{t} = 0$, $\partial/\partial\tilde{x} = 0$ and $\partial/\partial\tilde{y} = 0$. In this case the governing equations (2.16)–(2.18) simplify to

$$\frac{\mathrm{d}^2\tilde{u}}{\mathrm{d}\tilde{z}^2} = -Re_\tau\tilde{c} \quad \text{and} \quad -\tilde{V}_z\frac{\mathrm{d}\tilde{c}}{\mathrm{d}\tilde{z}} = \frac{1}{Re_\tau Sc}\frac{\mathrm{d}^2\tilde{c}}{\mathrm{d}\tilde{z}^2}. \tag{3.1}$$

Integrating (3.1) with boundary conditions (2.4)–(2.6) yields

$$\tilde{c} = A\exp(-\tilde{V}_z Re_\tau Sc\,\tilde{z}), \tag{3.2}$$

and

$$\tilde{u} = \frac{A}{\tilde{V}_z^2 Re_\tau Sc^2}\left[-\exp(-\tilde{V}_z Re_\tau Sc\tilde{z}) - Re_\tau\, \tilde{V}_z\, Sc\, \tilde{z}\exp(-\tilde{V}_z Re_\tau Sc) + 1\right]. \tag{3.3}$$

The constant A cannot be determined using the boundary conditions. The amount of sediments present in the flow at steady state depends on the initial condition. Thus, the system is closed with the criterion

$$\int_0^1 \tilde{c}\,\mathrm{d}\tilde{z} = 1, \tag{3.4}$$

which gives

$$A = \frac{\tilde{V}_z Re_\tau Sc}{1 - \exp(-\tilde{V}_z Re_\tau Sc)}. \tag{3.5}$$

The limiting case of $\tilde{V} = 0$ leads to a uniform concentration profile and a parabolic velocity profile

$$\tilde{u} = -\frac{Re_\tau}{2}(\tilde{z}^2 - 2\tilde{z}). \tag{3.6}$$

In the other limiting case of very large settling velocity, i.e. $\tilde{V} \to \infty$, the sediments settle to the bottom and the concentration profile is given by a Dirac delta function located at $\tilde{z} \to 0_+$. It can be shown from (3.3) that $\tilde{u}_{max} \to 0$ as $\tilde{V}_z \to \infty$, and therefore the flow ceases to exist. Figure 2 shows the laminar velocity and concentration profiles for $\tilde{V} = 0.0265$, $1/\tan\theta = 11.43$, $Re_\tau = 180$ and $Sc = 1$.

4. Results

As mentioned before, in turbidity currents suspended sediments play a dual role of both driving and stratifying the flow. Under extreme situations, stratification can lead to complete turbulence suppression. At this state, the flow loses its ability to keep sediments in suspension and it ceases to exist due to complete sedimentation. Previous research has highlighted the existence of a critical settling velocity beyond which complete turbulence suppression occurs (Cantero *et al.* 2009*a*,*b*), but the underlying mechanisms remain to be explored.

Table 1 lists all the different simulations analysed in this work to address the mechanism of turbulence damping in turbidity currents. Six different cases of stratified flows are considered. Cases 1–6 correspond to simulations where the settling velocity of sediments is increased from $\tilde{V} = 1 \times 10^{-2}$ to $\tilde{V} = 2.65 \times 10^{-2}$. Case 0, with $\tilde{V} = 0$, is the reference case, since its solution corresponds to unstratified turbulent channel flow driven by a uniform body force. As shown in figure 2(*a*), the concentration profile for case 0 is uniform. The corresponding velocity profile is shown in figure 2(*b*), and in figure 3 in wall units as $u^+ = \bar{u}/u_*$ versus $z^+ = zu_*/\nu$, where very good agreement is observed with the law of the wall ($u^+ = z^+$) for $z^+ < 5$ and with the log law ($u^+ = 1/0.41\log(z^+) + 5.5$) for $z^+ > 30$. Table 1 also reports cases S1 and S2, which correspond to flows where the stratification effect of suspended sediments is turned off by suppressing relevant terms in the momentum equation.

The results presented in this work represent long-term asymptotic stationary states (statistically steady states) of the flow. Two different initial conditions were considered in this study to address the sensitivity of the stationary state to the initial conditions:

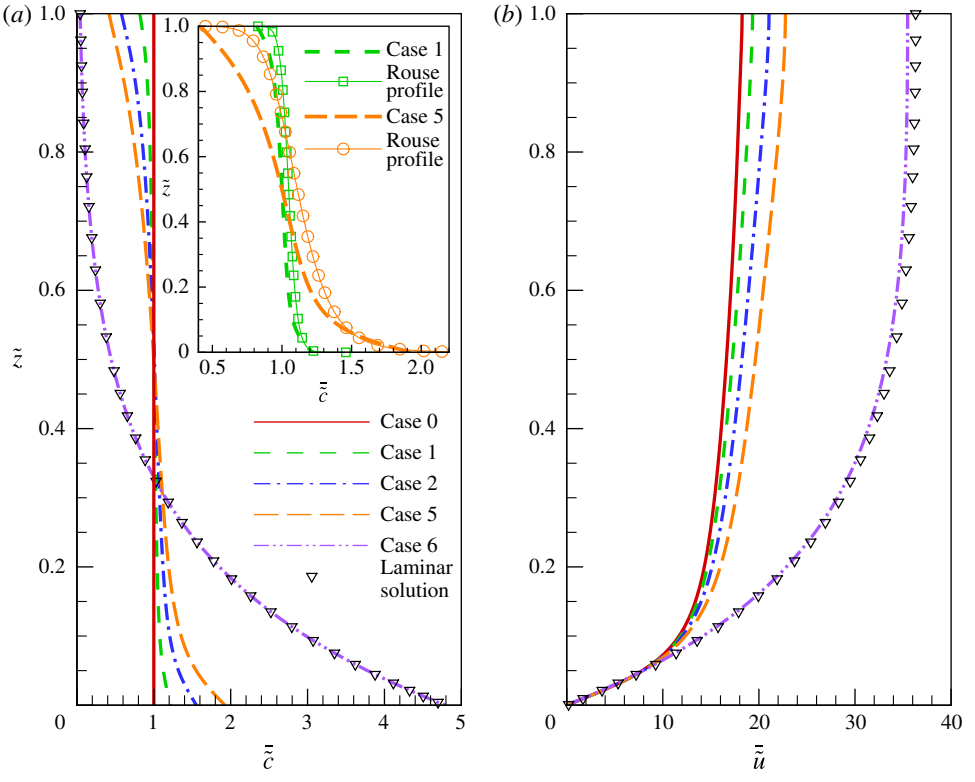

FIGURE 2. (Colour online) (*a*) Mean concentration profiles. (*b*) Mean velocity profiles. The laminar solution is computed for $\tilde{V} = 0.0265$, $1/\tan\theta = 11.43$, $Re_\tau = 180$ and $Sc = 1$ (same set of parameters for case 6). The inset in (*a*) compares mean concentration profiles for cases 1 and 5 with their Rouse profiles. Refer to (2.15) for the expression for Rouse profiles. It should be noted that κ in the expression of Rouse profiles is not the von Kármán constant but the modified constant based on best fit to the velocity log law. Refer to table 1 for values of κ.

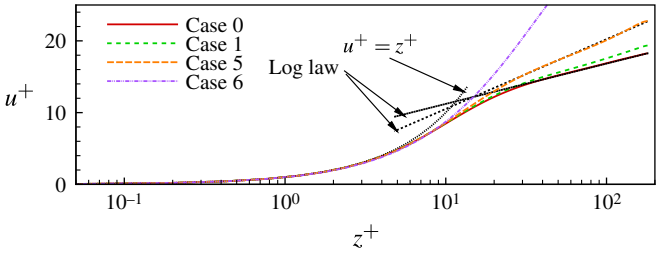

FIGURE 3. (Colour online) Mean velocity profiles in wall units. The two log laws shown correspond to best fit values presented in table 1 for cases 0 and 5.

(i) unstratified turbulent channel flow with uniform concentration of sediments (the stationary state of case 0); and (ii) an instantaneous velocity and concentration fields of a nearby turbulent case taken during its stationary state (for example, an instantaneous flow field of the stationary state of case 2 is used as initial condition for

case 3). Several of the cases in table 1 were simulated with these two initial conditions. It was observed that the approach to the stationary state from the initial condition is oscillatory. Quantities such as near-bed horizontally averaged concentration of sediments evolve from the initial condition to the final stationary value displaying overshoots and undershoots. The farther the initial condition is from the stationary value, the larger these overshoots and undershoots are. Furthermore, it is observed that the oscillatory behaviour of the solution has an impact on the final state only for the cases where the sediment settling velocity is just below the critical value for complete turbulence suppression (only case 5 in the present investigation). In this sense, the final asymptotic state can be taken to be insensitive to the precise initial condition employed. The results presented here for case 5, which falls in this small sensitive range, were obtained by minimizing the initial overshoot of the solution. The oscillatory behaviour of the solution at early times will not be discussed here.

4.1. *Mean values and turbulent fluxes in stratified flows*

The mean concentration profiles of selected cases given in table 1 are shown in figure 2(*a*). As the settling velocity of sediments increases, the resulting concentration profile no longer remains uniform and increasingly deviates from the reference profile of case 0. The resulting non-uniform mean concentration of sediments is skewed towards the bed, which affects the flow in two ways. First, the streamwise driving force, represented by the first term on the right-hand side of (2.21), is also correspondingly skewed towards the bed. Second, the stable stratification induced by concentration gradients tends to dampen turbulence, and this effect is captured by the last two terms on the right-hand side of (2.21). As will be discussed below, the effect of a skewed driving force is not as strong, and the stratification effect is the dominant mechanism responsible for complete turbulence suppression.

Figure 2(*a*) shows a clear change of regime from cases 5 to 6. While case 5 shows a well-mixed concentration profile, the concentration profile for case 6 is nearly zero in the top part of the channel and presents large values in the near-bed region. Corresponding mean velocity profiles are shown in figure 2(*b*), and they also show a clear change of regime from cases 5 to 6. While the velocity profile for case 5 shows a small deviation from the turbulent velocity profile of case 0, the velocity profile for case 6 shows less mixing and resembles a laminar profile. In the inset of figure 2(*a*) mean concentration profiles of cases 1 and 5 are compared with their corresponding Rouse profiles. Rouse profile (2.15) is an approximation for the concentration profile achieved by characterizing the turbulent mixing term in (2.9) by eddy diffusivity. Rouse profiles of cases 1 and 5 are evaluated using the modified von Kármán constant κ which is given in table 1. This quantifies the effect of stratification on the turbulent mixing in the channel. From the figure it is clear that Rouse profiles over-predict the turbulent mixing in stratified flows, leading to fuller concentration profiles. Figure 3 presents the velocity profiles in wall units on log-linear scales. Also included in this figure is the logarithmic law of the wall $u^+ = 1/\kappa \log(z^+) + B$ for cases 0 and 5 with adjusted constants. The best fit values of κ and B for all cases are listed in table 1. The velocity profiles for cases 0–5 show a definite turbulent nature with a definite logarithmic region for $z^+ > 30$. The deviation from the fully turbulent logarithmic law (case 0) is only in terms of the constant values. This change in the constants can be attributed to the damping of turbulence because of stratification (Cantero *et al.* 2009*a*). Case 6, on the other hand, does not display a logarithmic region. Figure 2(*a,b*) also shows the laminar solution computed for the same set of parameters used for case 6.

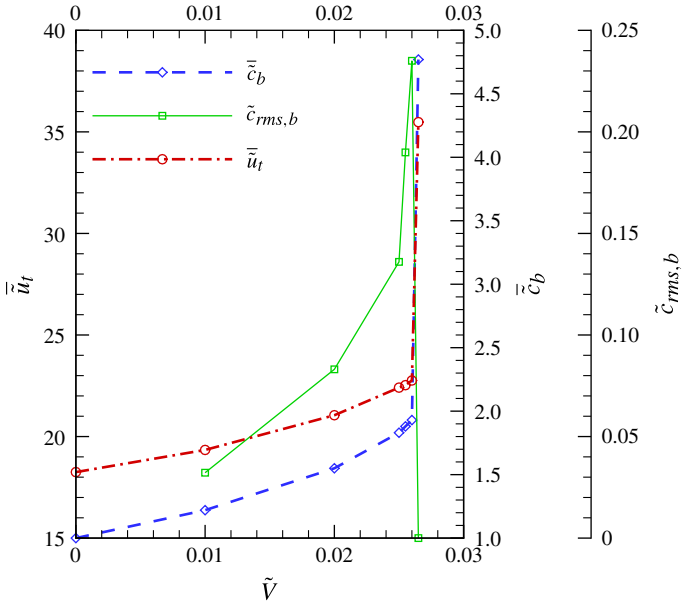

FIGURE 4. (Colour online) Variation in top mean velocity $\bar{\tilde{u}}_t$, mean concentration of sediments at the bed $\bar{\tilde{c}}_b$ and r.m.s. fluctuations of concentration of sediments at the bed $\tilde{c}_{rms,b}$ with settling velocity. There is a clear change of flow regime about the critical settling velocity which lies between the corresponding values for cases 5 and 6.

Almost perfect agreement is observed between case 6 and the corresponding laminar solution.

The nature of the change of flow regime can be further explored in figure 4, where the mean velocity at the top boundary ($\bar{\tilde{u}}_t$) and the mean concentration at the bed ($\bar{\tilde{c}}_b$) are plotted as a function of settling velocity of sediments. Below the critical value, increase in the settling velocity of sediments results in modest increase in the net flow rate, as indicated by the increase of the mean velocity at the top stress-free boundary. Around the critical settling velocity there is an abrupt increase in $\bar{\tilde{u}}_t$ signalling the change of flow regime. A similar behaviour can also be observed in the mean concentration of sediments at the bed, which increases slowly for below-critical values of settling velocity. Across the critical value, an abrupt increase in the bottom concentration can be observed.

The balance between the settling flux of sediments ($\tilde{V}_z\bar{\tilde{c}}$) and the turbulent flux of sediments ($\overline{\tilde{w}'\tilde{c}'}$) can be obtained from (2.9) as

$$\tilde{V}_z\bar{\tilde{c}} = \overline{\tilde{c}'\tilde{w}'} - \frac{1}{Re\,Sc}\frac{\mathrm{d}\bar{\tilde{c}}}{\mathrm{d}\tilde{z}}. \tag{4.1}$$

Increase in the settling velocity increases the settling flux of sediments. In order to keep the sediments well mixed in the flow ($\mathrm{d}\bar{\tilde{c}}/\mathrm{d}\tilde{z} \approx 0$), there must be a proportional increase in the turbulent flux of sediments. In other words, in a well-mixed channel the ratio of turbulent flux to settling flux of sediments approaches 1. The relative importance of turbulent flux of sediments can be seen in figure 5(*a*), which shows the variation of the ratio of turbulent flux to settling flux in the bed-normal direction. From figure 5(*a*) it is evident that the increase in turbulent flux is not proportional

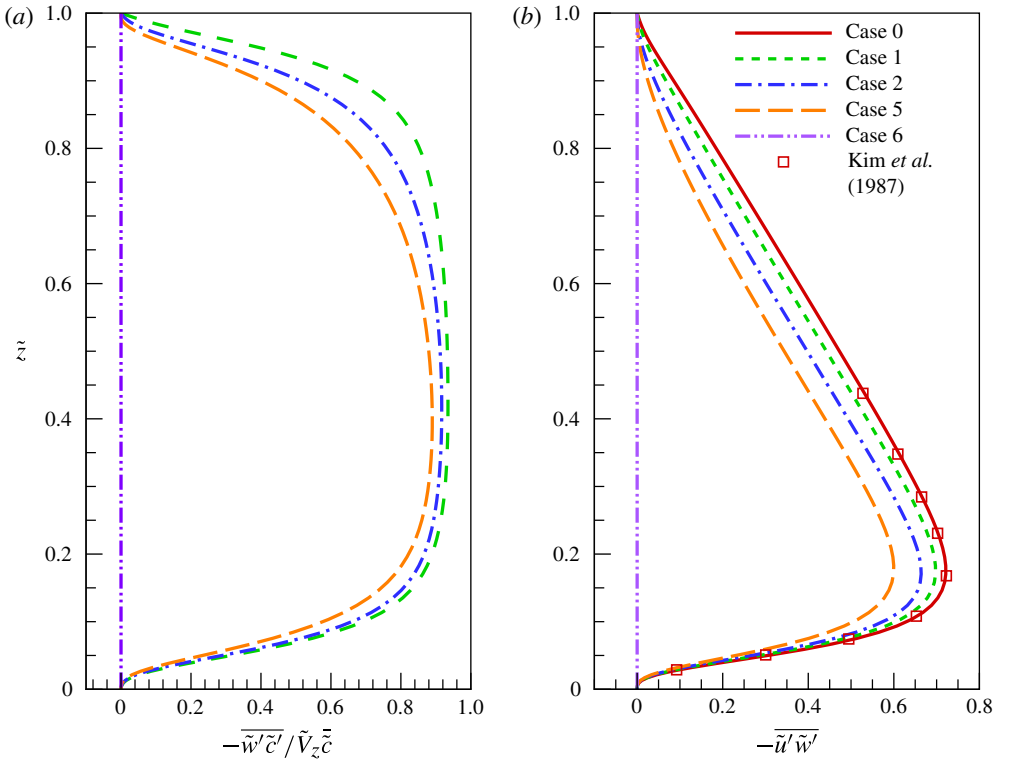

FIGURE 5. (Colour online) (*a*) Profiles of the ratio of sediment turbulent flux to settling flux. (*b*) Profiles of Reynolds stress. Results from Kim, Moin & Moser (1987) are also plotted to validate case 0.

to settling flux for all the cases shown. This ratio shows a decreasing trend with increasing settling velocity of sediments, but the decrease is not very sensitive for cases 1–5. Also, the decrease is not uniform throughout the channel: it is more pronounced near the top boundary than near the bed. This asymmetry is due to reduction of turbulent transport from near the bed, where turbulence production occurs, to the upper part of the channel. For case 6 the turbulent flux of sediments is zero. This trend shows the effect of stratification but it cannot explain the sudden transition seen at the critical settling velocity.

Figure 5(*b*) shows profiles of the Reynolds stress $\overline{\tilde{u}'\tilde{w}'}$. For cases 1–5 the small reduction in Reynolds stress with increase in settling velocity of sediments suggests that the effect of stratification is weak. However, with further increase in settling velocity of sediments above the critical value, a dramatic shut-off is seen in the Reynolds stress. The corresponding DNS results of Kim *et al.* (1987) for pure channel flow are also shown in figure 5(*b*). The perfect agreement with the results for case 0 serves as validation of the simulation procedure and the resolution employed in this work.

Turbulent intensity or root mean square (r.m.s.) velocity fluctuations ($\tilde{u}_{rms} = \sqrt{\overline{\tilde{u}'^2}}$) are shown in figure 6. The variation of all r.m.s. velocity fluctuations is very small for cases 1–5. For case 6, $\tilde{w}_{rms}$ and $\tilde{v}_{rms}$ are zero, while the streamwise velocity fluctuations $\tilde{v}_{rms}$ are finite but small. Thus, for case 6 the stratification

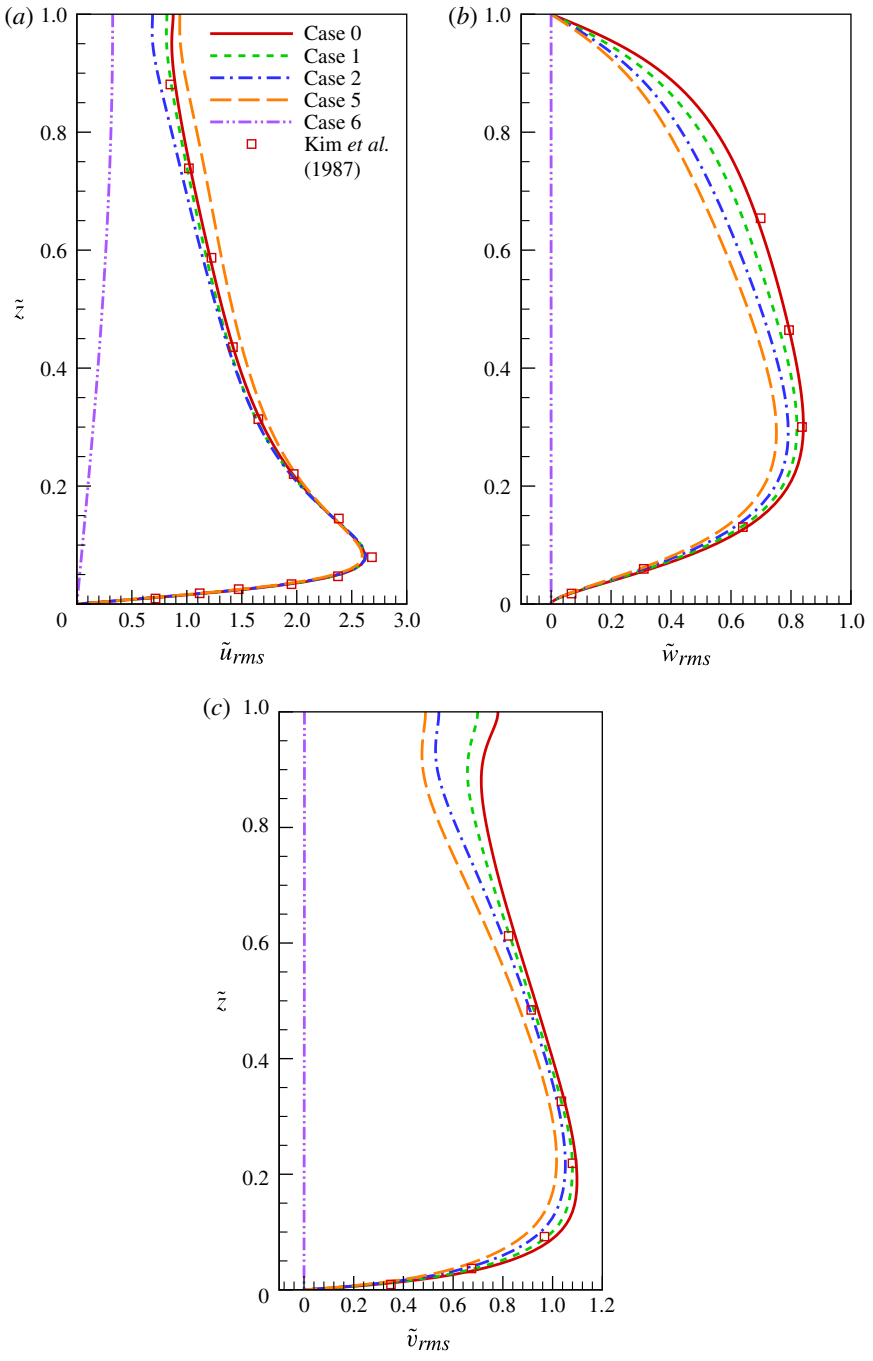

FIGURE 6. (Colour online) Profiles of r.m.s. velocity fluctuations: (*a*) $\tilde{u}_{rms}$; (*b*) $\tilde{w}_{rms}$; (*c*) $\tilde{v}_{rms}$. Corresponding profiles from Kim *et al.* (1987) are also presented as validation for case 0.

effects are successful in completely suppressing the wall-normal and spanwise velocity fluctuations and thereby all wall-normal and spanwise momentum and mass transport.

However, some sheet-like streamwise velocity fluctuations persist, contributing to $\tilde{u}_{rms}$. Again, the corresponding DNS results of Kim *et al.* (1987) for unstratified channel flow are also shown in figure 6, which are in perfect agreement with the results for case 0.

These results lead to the viewpoint that there exists a critical value for settling velocity of sediments, and even a small increase beyond this value will cause a sudden change in the flow regime. It will be shown in the following sections that the flow for cases 1($\tilde{V}_s = 0.01$)–5 ($\tilde{V}_s = 0.026$) remains turbulent, while case 6 ($\tilde{V}_s = 0.0265$) undergoes complete turbulence suppression.

4.2. *Isolated effects of non-uniform streamwise forcing*

One of the effects of settling sediments is to focus the driving force close to the bed. In order to understand the isolated effect of the non-uniform driving force on flow turbulence, some simulations were performed where the stratification effect on the flow is turned off. This is achieved by neglecting the body force term (the last two terms in (2.21)) in the bed-normal (z-direction) momentum equation. These simulations are listed in table 1 as cases S1 and S2. The settling velocity of sediments in case S1 is exactly the same as case 3 and therefore their results can be compared to understand the effect of stratification on turbulent flows. As will be shown in this section, the abrupt suppression of turbulence in the flow does not occur without the influence of stratification. In order to clearly demonstrate this feature, case S2 considers sediments with large settling velocity of nearly four times the critical settling velocity for complete turbulence suppression identified in the previous section.

In figure 7(*a,b*) the mean concentration and mean velocity profiles for the cases S1 and S2 are compared with those of cases 0 and 3. Case 0 corresponds to a uniform driving force and serves as the reference case. As can be expected, with increasing settling velocity the mean concentration profiles also skew toward the bed for cases S1 and S2. The skewness of these profiles is, however, smaller than that of the profiles in figure 2(*a*). Since the total volume-averaged concentration of sediments is constrained to be a constant, the total streamwise driving force remains the same in all cases, but the strong bed-normal variation in the streamwise driving force for case S2 is reflected in its concentration profile. Concentration profiles of cases S1 and S2 are also compared with their corresponding Rouse profiles (2.15) in the inset of figure 7(*a*). The Rouse profiles show higher gradients as compared to the corresponding profiles obtained from the DNS. This suggests that Rouse profiles under-predict the amount of turbulent mixing in these cases.

The isolated effect of the skewed driving force on the mean turbulent velocity profile is shown in figure 7(*b*). In all the cases listed in table 1 the dimensionless velocity gradient at the bottom boundary is Re_τ by the definition of u_* (see (2.12)). As seen in figure 7(*b*) for cases S1 and S2, the effect of skewed forcing is to make the velocity profile fuller by reducing the velocity gradient away from the bed. The corresponding bulk velocity for cases S1 and S2 slightly increases with settling velocity (see table 1). On the other hand, the mean streamwise velocity at the top (location of the maximum value) slightly decreases. Nevertheless, the isolated effect of skewed driving force on the mean velocity profiles is negligible when compared to the effect of stratification seen for case 3 in figure 7(*b*) and for all cases shown in figure 2(*b*).

As mentioned previously, in order to keep the sediments well mixed in the channel the ratio of turbulent flux to settling flux of sediments must approach one. Figure 8(*a*) shows the ratio of turbulent flux to settling flux of sediments for cases S1, S2 and 3.

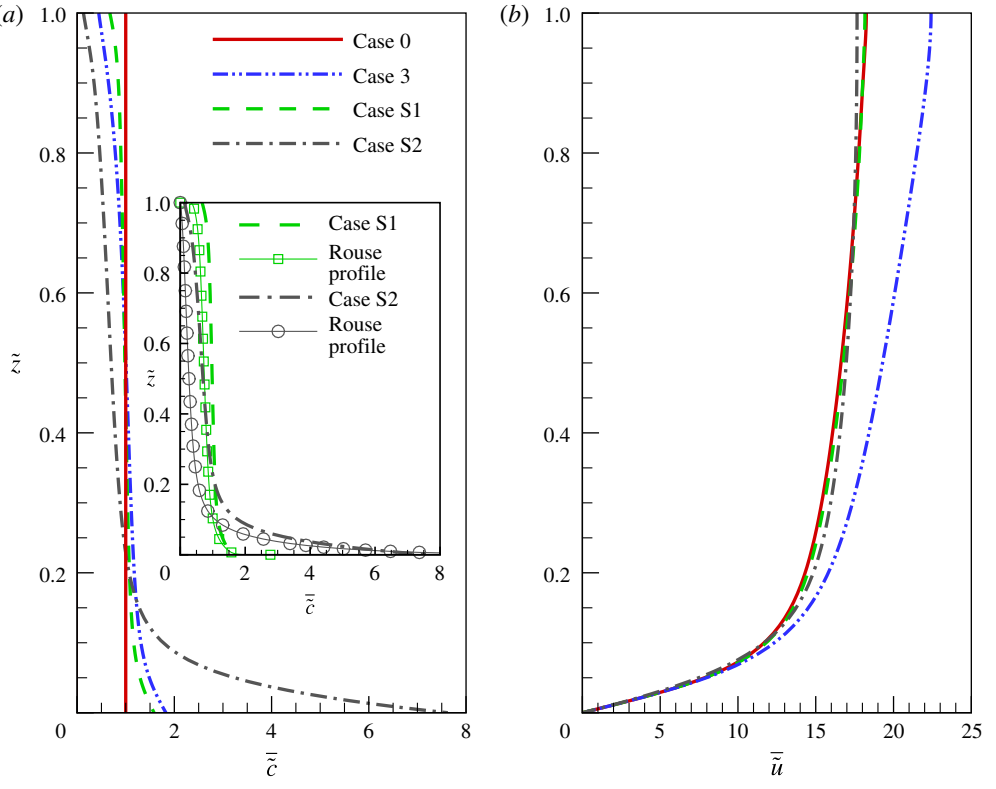

FIGURE 7. (Colour online) (*a*) Mean concentration profiles. (*b*) Mean velocity profiles. Cases S1 and S2 do not consider stratification effects. The inset in (*a*) shows the Rouse profiles for cases S1 and S2. Refer to (2.15) for the expression of Rouse profiles. Again κ in the expression of Rouse profiles is not the von Kármán constant but the modified constant based on best fit to the velocity log law. Refer to table 1 for values of κ.

It can be observed in this figure that the ratio is larger for cases S1 and S2 than for case 3, and very close to one. Specifically, for case S2 the ratio practically reaches unity close to the centre of the channel. The ratio decreases and reaches zero at the boundaries by definition of turbulent fluxes. Similar behaviour can be seen in figure 8(*b*), where the streamwise r.m.s. velocity fluctuations are shown. The damping effect is negligible for case S1. A decrease of $\sim$10 % can be observed in the peak value for case S2. This effect, however, can also be considered to be minor when compared to case 6 in figure 6(*a*). Similar behaviours are observed for spanwise and bed-normal r.m.s. velocity fluctuations and are not shown here.

These results show clearly that turbulent mixing is fully active for cases S1 and S2, thus reinforcing the idea that the isolated effect of skewed driving force on turbulence damping is negligible as compared to the effect of stratification. The focusing of the driving force close to the bed induces a modest reduction in the turbulent intensities, but the turbulent nature and mixing capability of the flow prevail. With significantly larger settling velocities than that of case S2, as the driving force moves very close to the bed, where the viscous effects dominate, total suppression of turbulence could still be achieved even in the absence of stratification effects.

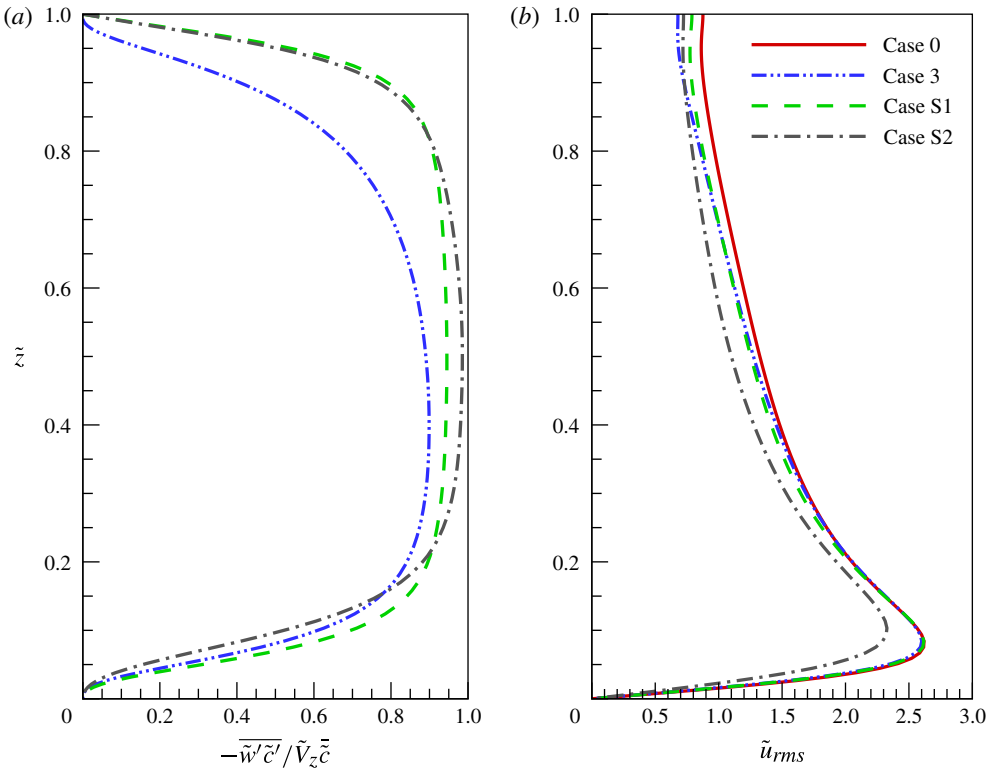

FIGURE 8. (Colour online) (*a*) Ratio of sediment turbulent flux to settling flux. (*b*) Profiles of streamwise r.m.s. velocity fluctuations. Cases S1 and S2 do not consider stratification effects.

4.3. *Turbulent kinetic energy balance*

The dimensionless turbulent kinetic energy (TKE) equation for the present statistically stationary and horizontally homogeneous flow can be expressed as

$$\tilde{\mathscr{P}} - \tilde{\epsilon} + \frac{\mathrm{d}}{\mathrm{d}\tilde{z}}\left[\frac{1}{Re_\tau}\frac{\mathrm{d}\tilde{k}}{\mathrm{d}\tilde{z}} - \overline{\tilde{w}'\left(\tilde{p}' + \frac{1}{2}\tilde{u}_i'\tilde{u}_i'\right)}\right] = -\tilde{F}_x + \frac{\tilde{F}_z}{\tan\theta}, \tag{4.2}$$

where the TKE $\tilde{k}$, the TKE production $\tilde{\mathscr{P}}$, the TKE dissipation $\tilde{\epsilon}$, and the turbulent flux of sediments $\tilde{F}_i$ are expressed as

$$\tilde{k} = \frac{1}{2}\overline{\tilde{u}_i'\tilde{u}_i'}, \quad \tilde{\mathscr{P}} = -\overline{\tilde{u}_i'\tilde{u}_j'}\frac{\partial\bar{\tilde{u}}_i}{\partial\tilde{x}_j}, \quad \tilde{\epsilon} = \frac{1}{Re_\tau}\overline{\frac{\partial\tilde{u}_i'}{\partial\tilde{x}_j}\frac{\partial\tilde{u}_i'}{\partial\tilde{x}_j}}, \quad \tilde{F}_i = \overline{\tilde{u}_i'\tilde{c}'}. \tag{4.3}$$

Figure 9(*a,b*) shows profiles of TKE production and dissipation for selected cases in table 1. Production has a pronounced peak close to the bed. For case 0 the peak is at $\tilde{z} = 0.067$, which corresponds to $z^+ \sim 12$, and its dimensionless value is ∼40, which correspond well to reported results for unstratified channel flow (Kim *et al.* 1987). The influence of non-zero settling velocity on the location of production peak is small: the peak tends to slightly shift away from the bed. Also, the peak value of production is seen to decrease with increase in settling velocity of sediments. There is ∼13 % reduction in production peak from cases 0 to 5. Two regions of opposite trends can be

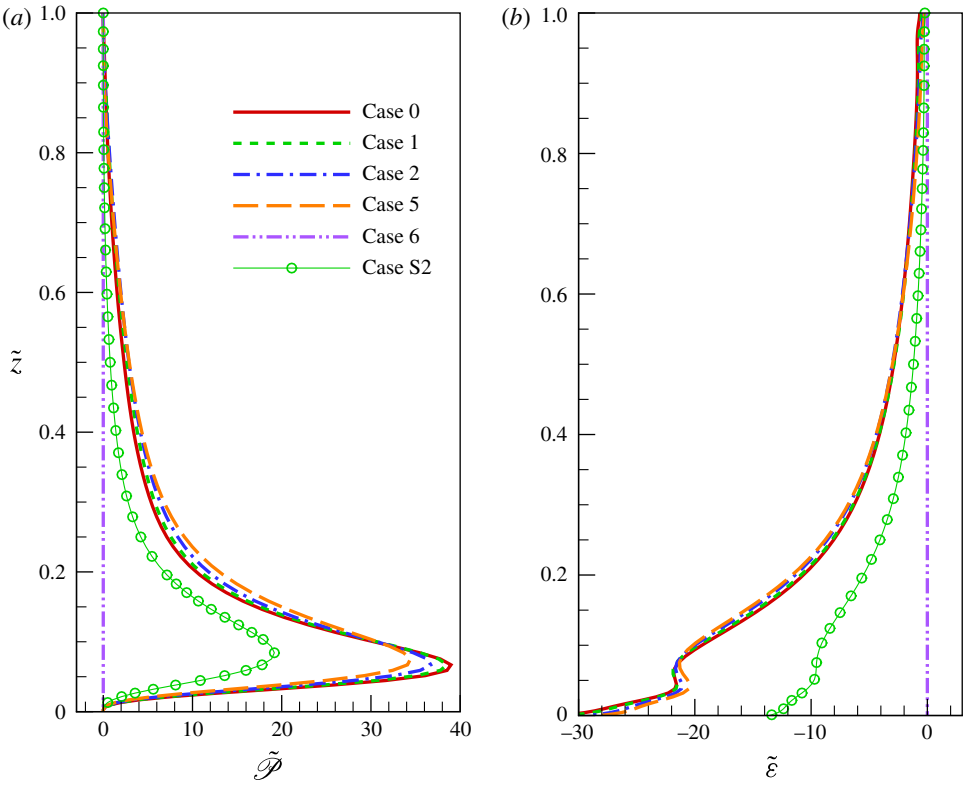

FIGURE 9. (Colour online) (*a*) Turbulent kinetic energy shear production. (*b*) Turbulent kinetic energy dissipation.

observed in figure 9(*a*). In the region between the bed and $\tilde{z} \sim 0.1$ there is damping of TKE production with increase in settling velocity of sediments. Beyond this location ($\tilde{z} > 0.1$) rise in the TKE production is observed with increase in settling velocity of sediments. The influence of stratification caused by suspended sediments on the TKE dissipation is not as pronounced as for production.

Figure 9(*a,b*) shows the results for case 6, which corresponds to currents driven by sediments with supercritical settling velocity. Both TKE production and dissipation are identically zero throughout the channel. Also plotted in these figures are the results for case S2 corresponding to the larger settling velocity with stratification effects turned off. Consistent with the other turbulent quantities, some reduction in both TKE production and dissipation is observed, but the flow still remains vigorously turbulent.

The contribution of the suspended sediments to the TKE budget (right-hand side terms in (4.2)) is plotted in figure 10(*a*). Suspended sediments act as a sink and damp TKE. This amount of TKE is expended in keeping the sediments suspended. Figure 10(*a*) shows that TKE damping, induced due to sediments, peaks near the bed at about the location where the TKE production peaks, but the peak is broader as the decay of TKE damping away from the peak into the channel is slower than the TKE production. This behaviour can be clearly seen in figure 10(*b*), where the ratio of TKE damping to TKE production is shown. The ratio is only a few per cent in the region

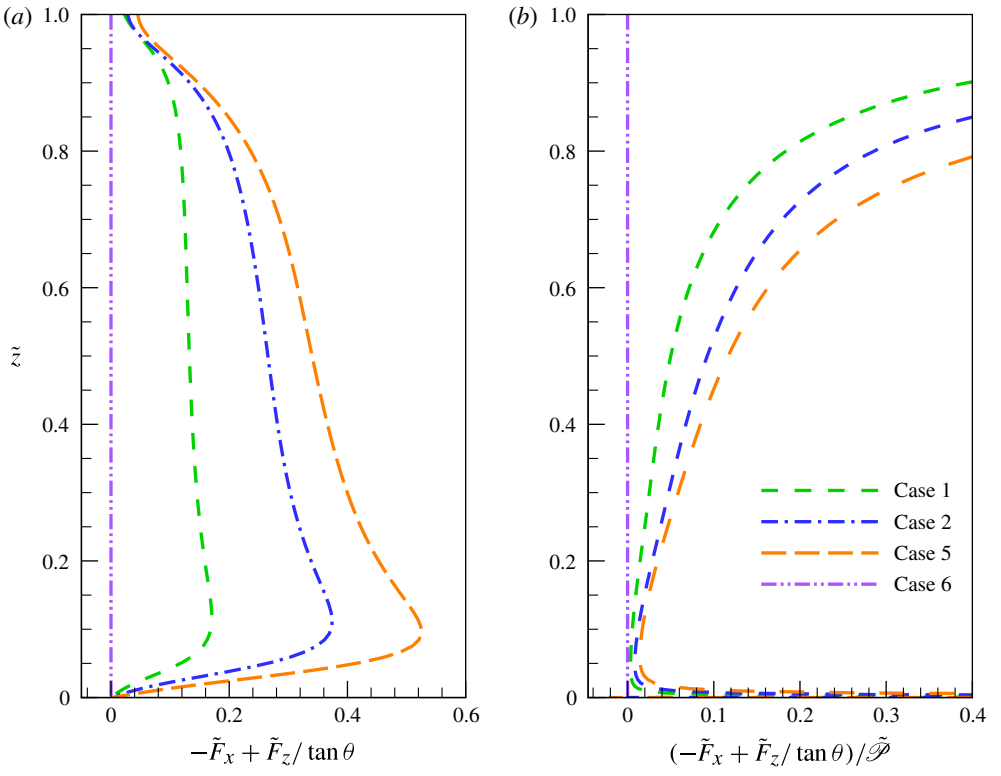

FIGURE 10. (Colour online) (*a*) Sediment-induced damping terms in the turbulent kinetic energy budget. (*b*) Ratio of sediment-induced damping to production of turbulent kinetic energy (TKE).

where both the production and damping peak, but larger away from the peak where production becomes very small.

The global balance of TKE in the flow can be obtained by integrating (4.2) in the bed-normal direction,

$$\tilde{P} - \tilde{\varepsilon} + \frac{1}{Re_\tau}\left\{\left[\frac{\mathrm{d}\tilde{k}}{\mathrm{d}\tilde{z}}\right]_0^1 + \frac{\zeta}{\tan\theta}\right\} = \beta + \frac{\tilde{V}_z}{\tan\theta}, \tag{4.4}$$

where we have used the fact that $\tilde{F}_z = \overline{\tilde{w}'\tilde{c}'} = \tilde{V}_z\bar{\tilde{c}} + 1/(Re_\tau Sc)\,\mathrm{d}\bar{\tilde{c}}/\mathrm{d}\tilde{z}$ (refer to (4.1)), and

$$\tilde{P} = \int_0^1 \tilde{\mathscr{P}}\,\mathrm{d}\tilde{z}, \quad \tilde{\varepsilon} = \int_0^1 \tilde{\epsilon}\,\mathrm{d}\tilde{z}, \quad \beta = -\int_0^1 \overline{\tilde{u}'\tilde{c}'}\,\mathrm{d}\tilde{z}, \quad \zeta = \frac{\bar{\tilde{c}}_b - \bar{\tilde{c}}_t}{Sc}. \tag{4.5}$$

Here $\bar{\tilde{c}}_t$ and $\bar{\tilde{c}}_b$ are the mean concentration on the top boundary and bed, respectively. The first two terms on the left-hand side of (4.4) are the bulk TKE production and the bulk TKE dissipation. The two terms on the right-hand side of (4.4) are the bulk sediment-induced damping of TKE and represent the total amount of TKE spent to keep the sediments suspended and well mixed in the bed-normal direction. The term β arises from the term $\tilde{F}_x$ in (4.2). The second damping term is the manifestation of

Case	$\tilde{k}$	$\tilde{P}$	$\tilde{\varepsilon}$	β	$\tilde{V}_z/\tan\theta$	$\zeta/(Re_\tau\tan\theta)$	$\beta\tan\theta/\tilde{V}_z$	$(\tilde{V}_z/\tan\theta+\beta)/\tilde{P}$
1	1.71	6.34	6.04	0.0358	0.114	0.0254	0.31	0.024
2	1.62	6.54	6.27	0.0772	0.228	0.0619	0.34	0.046
3	1.58	6.57	6.23	0.1040	0.285	0.0877	0.36	0.059
4	1.64	6.54	6.20	0.1100	0.291	0.0918	0.38	0.061
5	1.71	6.59	6.23	0.1170	0.296	0.0958	0.40	0.063

TABLE 2. Turbulent kinetic energy budget of cases listed in table 1.

the $(\tilde{F}_z/\tan\theta)$ term in (4.2). The last term on the left-hand side of (4.4) comprises two effects: bulk diffusion of TKE and bulk hydrodynamic diffusion of sediments. For large Reynolds numbers this term becomes negligible as compared to the other terms in the budget.

The terms involved in the global balance of TKE are shown in table 2. As seen from the table, there are two terms which contribute to TKE production. These terms are the TKE production $\tilde{P}$, and the bulk hydrodynamic sediment–sediment and sediment–bed interactions $(\zeta/(Re_\tau\tan\theta))$. Although the introduction of $(\zeta/(Re_\tau\tan\theta))$ into the bulk TKE equation is through a damping term $\tilde{F}_z$, from its contribution to the balance it can be thought of as a mechanism that supports TKE. At large Reynolds numbers, however, this term becomes negligible. Table 2 shows that the sediment-induced damping terms amount to only 2–6 % of the TKE production. Observe that for case 5 the sediment-induced damping of TKE is 6.3 %, while for case 6, with a settling velocity only 2 % larger than case 5, the sediment-induced damping of TKE is complete.

The term β is ∼30–40 % of $(\tilde{V}_z/\tan\theta)$ over the range of settling velocities considered. Assuming that the scaling of β with $(\tilde{V}_z/\tan\theta)$ remains valid over a wide range of Reynolds numbers of practical interest, then the overall suspended-sediment-induced TKE damping can be expressed as some factor of $(\tilde{V}_z/\tan\theta)$. Thus, the entire damping process can be represented by the parametric combination of slope of the channel (θ) and settling velocity of the sediments $(\tilde{V}_z)$, and the combination takes the form $\tilde{V}_z/\tan\theta$. Recently, Cantero, Shringarpure & Balachandar (2012*b*) have suggested that there exists a universal criterion for total turbulence suppression. The authors have identified that the extent of turbulence damping can be quantified based on the parametric grouping of settling velocity of sediments (V_z) and slope of the channel (θ), which combine to give $\tilde{V}_z/\tan\theta$. Therefore, at any given Re_τ there exists a critical value of $\tilde{V}_z/\tan\theta$ beyond which complete turbulence suppression occurs. This also means that for sediments of a certain settling velocity there exists a critical value for channel slope below which complete turbulence suppression occurs. Cantero *et al.* (2012*a*) and Talling *et al.* (2007) have shown that a change in the slope of the channel can result in complete suppression of turbulence, leading to massive sedimentation.

It is very intriguing that complete turbulence suppression could be abruptly produced by the small values of sediment-induced TKE damping shown in table 2. What causes the collapse of turbulence and how the damping terms initiate the process of complete turbulence suppression are the core questions.

4.4. *Energy spectra*

In order to explore the dependence of suspended sediments and their dominant stratification effect on flow scales, the x and y energy spectra of the streamwise,

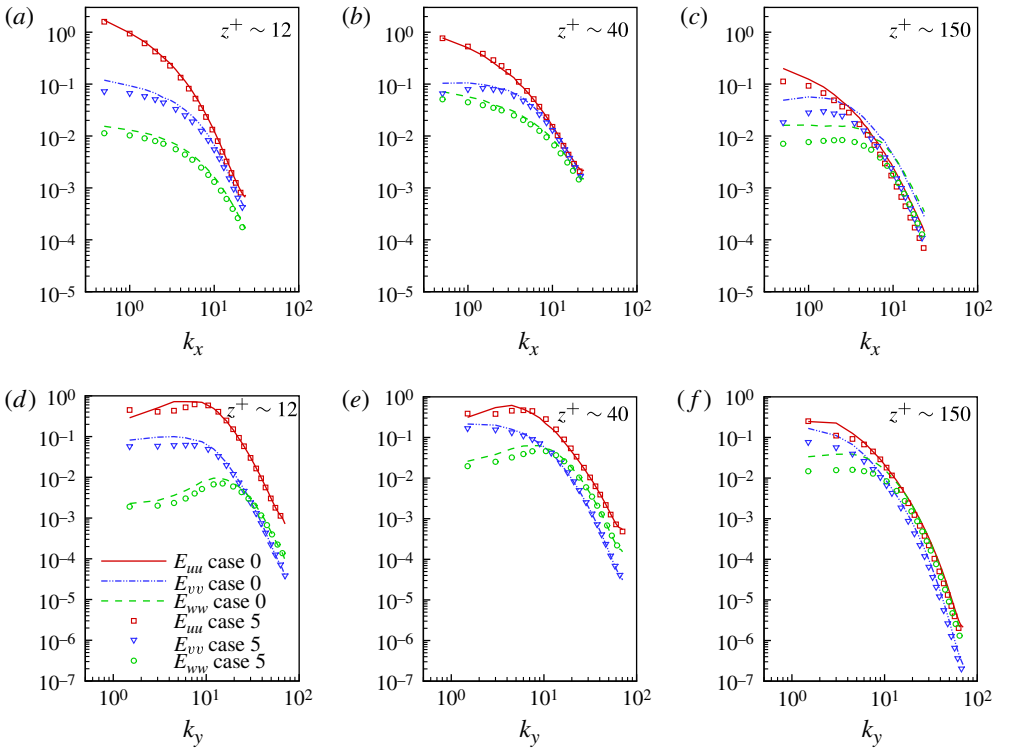

FIGURE 11. (Colour online) Energy spectra at $z^+ \sim 12$ (buffer layer), $z^+ \sim 40$ (logarithmic layer) and $z^+ \sim 150$ (away from the bed): (*a–c*) *x*-direction spectra, (*d–f*) *y*-direction spectra.

spanwise and bed-normal components of velocity are considered. Comparing the energy spectra of cases 0 and 5 (reference case and largest settling velocity before complete turbulence suppression, respectively) gives an idea of the level to which the different scales of turbulence are influenced by the suspended sediments. Figure 11 presents the energy spectra of all the components of velocity at three different distances away from the bed: $z^+ \sim 12$ (buffer layer), $z^+ \sim 40$ (logarithmic layer) and $z^+ \sim 150$ (away from the bed). Figures 11(*a*)–11(*c*) correspond to *x*-spectra and figures 11(*d*)–11(*f*) correspond to *y*-spectra. It is worth noticing that all the spectra show several decades of energy decay, indicating adequate spatial resolution of the entire range of turbulent scales.

Close to the bed (buffer and logarithmic layers) the *x*-spectra of streamwise velocity ($E_{uu}(k_x)$) for cases 0 and 5 virtually overlap, suggesting very little influence of suspended sediments. In contrast, the *x*-spectra of spanwise and bed-normal components of velocity ($E_{vv}(k_x)$ and $E_{ww}(k_x)$) are damped over all wavenumbers in these regions. The level of damping is somewhat larger for $k_x < 7$. The *y*-spectra show subtle differences with respect to the *x*-spectra in the buffer and logarithmic layers. For low wavenumbers ($k_y < 10$), $E_{vv}(k_y)$ and $E_{ww}(k_y)$ display similar influence from suspended sediments while a slight damping is seen for $\tilde{E}_{uu}(k_y)$. For high wavenumbers ($k_y > 10$), negligible damping is observed for all three energy spectra.

Away from the bed ($z^+ > 150$), the influence of suspended sediments on the energy spectra is more substantial. The *x*-spectra and *y*-spectra of all three velocity

components show significant reduction in the energy content for case 5. The general trend observed in the regions close to the bed prevails. That is, the effect of suspended sediments is more pronounced for the spanwise and bed-normal velocity components than for the streamwise component and the decay is more pronounced at lower wavenumbers than at higher wavenumbers.

The following deductions can be made from the energy spectra. First and foremost, stratification affects the large and moderate scale eddy structures of the flow more than the small (Kolmogorov) scale eddies. Also, the energy content of the spanwise and bed-normal velocity fluctuations is damped much more than the streamwise component, suggesting that stratification has a stronger effect on streamwise oriented vortical structures. Since turbulence production predominantly occurs in the region of the buffer layer, it can be argued that while stratification has a direct influence on turbulence production at the large and intermediate scale motions in the near-bed region, it also has a strong effect on turbulence transport to the upper regions of the flow, which results in substantial reduction in the spectra of all three velocity components in the region away from the bed. The process of complete turbulence suppression starts with damping of the large and intermediate scale eddies in the near-bed region, where the source of sustaining turbulence lies. By damping such eddies, the turbulence generation mechanisms are overpowered and eventually lead to the observed abrupt turbulence suppression. Section 4.7 will focus on turbulent flow structures to support this hypothesis and show that the mechanism responsible for complete turbulence suppression is the damping of near-bed streamwise oriented eddies.

4.5. *Reynolds stress balance*

The puzzling aspect of the observed complete turbulence suppression is its abrupt onset with increasing settling velocity of sediments. In fact, as was shown in table 2, just prior to onset of complete turbulence suppression, the sediment-induced damping of TKE accounts for only a few per cent of TKE production. Since Reynolds stress $\overline{\tilde{u}'\tilde{w}'}$ plays a crucial role in TKE production, this section further probes into how Reynolds stress balance and distribution are influenced by increasing the settling velocity of sediments.

For the present problem, the stationary state of the Reynolds stress balance in dimensionless form can be expressed as

$$\tilde{P}_{rey} - \tilde{\Phi}_{13} + \frac{\partial \overline{\tilde{u}'\tilde{w}'\tilde{w}'}}{\partial \tilde{z}} + \tilde{\Pi}_{13} - \frac{1}{Re_\tau}\frac{\partial^2 \overline{\tilde{u}'\tilde{w}'}}{\partial \tilde{z}^2} = -\frac{\tilde{F}_x}{\tan\theta} + \tilde{F}_z, \tag{4.6}$$

where

$$\tilde{P}_{rey} = \overline{\tilde{w}'\tilde{w}'}\frac{\partial \tilde{\bar{u}}}{\partial \tilde{z}}, \quad \tilde{\Phi}_{13} = -2\overline{\frac{\partial \tilde{u}_1'}{\partial \tilde{x}_j}\frac{\partial \tilde{u}_3'}{\partial \tilde{x}_j}}, \quad \tilde{\Pi}_{13} = \left\{ \overline{\tilde{w}'\frac{\partial \tilde{p}'}{\partial \tilde{x}}} + \overline{\tilde{u}'\frac{\partial \tilde{p}'}{\partial \tilde{z}}} \right\}. \tag{4.7}$$

The first term on the left-hand side is production, the second term is dissipation, and the last three terms are the turbulent, pressure and viscous transport. The terms on the right-hand side are the sediment-induced damping of Reynolds stress. These damping terms arise out of the fluctuations in concentration and velocity fields.

Figure 12 shows the Reynolds stress production and sediment-induced damping for selected cases from table 1. Reynolds stress production is not strongly influenced by settling velocity of sediments. The production peak remains nearly the same. Interestingly enough, Reynolds stress production slightly increases away from the peak

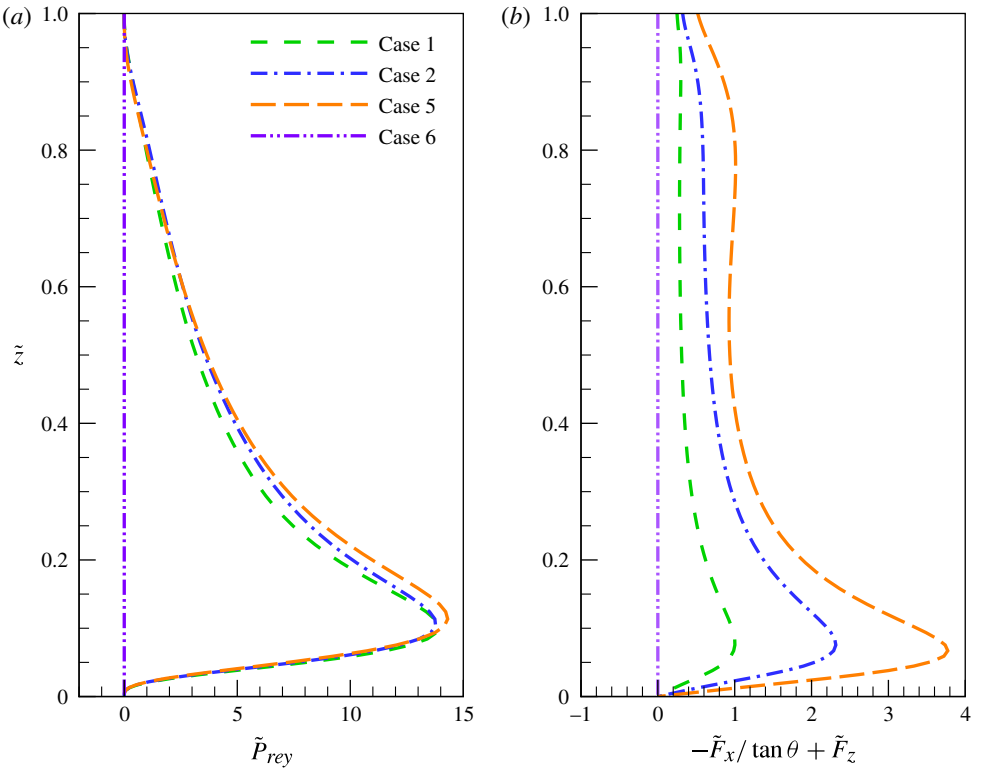

FIGURE 12. (Colour online) (*a*) Reynolds stress production. (*b*) Sediment-induced damping of Reynolds stress.

with increasing settling velocity of sediments. This can be explained by observing that production depends on both the r.m.s. bed-normal velocity fluctuations $\tilde{w}_{rms}$ and the mean velocity gradient $\partial\overline{\tilde{u}}/\partial\tilde{z}$. While $\tilde{w}_{rms}$ decreases with increasing sediment settling velocity, the corresponding mean velocity gradient increases to compensate. In contrast, the sediment-induced damping of Reynolds stress shows significant increase with increasing settling velocity of sediments.

The global balance of Reynolds stress in the channel is obtained by integrating the Reynolds stress equation (4.6) in the bed-normal direction,

$$\chi - \int_0^1 \left(\tilde{\Phi}_{13} - \tilde{\Pi}_{13}\right) \mathrm{d}\tilde{z} + \frac{1}{Re_\tau}\left\{-\left[\frac{\mathrm{d}\overline{\tilde{u}'\tilde{w}'}}{\mathrm{d}\tilde{z}}\right]_0^1 + \zeta\right\} = \frac{\beta}{\tan\theta} + \tilde{V}_z, \tag{4.8}$$

where

$$\chi = \int_0^1 \tilde{P}_{rey}\,\mathrm{d}\tilde{z}.$$

Here again, (4.1) has been used to rewrite $\tilde{F}_z$ or $\overline{\tilde{c}'\tilde{w}'}$ as $\tilde{V}_z\overline{\tilde{c}} + 1/(Re_\tau Sc)\,\partial\overline{\tilde{c}}/\partial z$. The terms involved in the bulk Reynolds stress balance are tabulated in table 3. Clearly, the most important sediment-induced damping term is $\beta/\tan\theta$. Observe that $\tilde{V}_z$ is $\sim$2 % of $\beta/\tan\theta$ for all cases considered. As in the TKE balance, ζ is a production

Case	χ	$\tilde{V}_z$	$\beta/\tan\theta$	ζ/Re_τ	$\tilde{V}_z \tan\theta/\beta$	$(\tilde{V}_z+\beta/\tan\theta)/\chi$
1	4.24	0.01	0.412	0.00222	0.024	0.099
2	4.53	0.02	0.880	0.00543	0.022	0.20
3	4.57	0.025	1.186	0.00767	0.021	0.265
4	4.61	0.0255	1.254	0.00803	0.020	0.28
5	4.68	0.026	1.330	0.00840	0.020	0.29

TABLE 3. Reynolds stress budget of cases listed in table 1.

term. Therefore, the sediment-induced damping of Reynolds stress is represented by $\beta/\tan\theta + \tilde{V}_z$. Unlike in the TKE balance, here the sediment-induced damping of Reynolds stress for case 5 is $\sim$30 % of production. The fractional damping of Reynolds stress by sediments is much stronger than the damping of TKE. Thus, the pathway to turbulence suppression is perhaps through modulation of Reynolds stress producing turbulent events.

4.6. *Reynolds stress events*

Recent research efforts (Bernard, Thomas & Handler 1993; Brooke & Hanratty 1993; Zhou, Adrian & Balachandar 1996; Zhou *et al.* 1999) have begun to shed light on how turbulence sustains itself even in a perfectly smooth-walled channel. One of the proposed mechanisms relies on the auto-generation of vortical structures and their arrangement as streamwise aligned packets (Zhou *et al.* 1996, 1999). Hairpin and other quasi-streamwise vortices in a turbulent wall layer generate secondary, tertiary and additional vortical structures over time only when their amplitude is above a certain threshold. The implication is that if the strength of the vortical structures falls below a certain threshold they lose their ability to generate the next generation of vortical structures and thus fail to sustain turbulence.

This line of argument is pursued in this section to explore the effect of suspended sediments on the typical Reynolds stress producing events. For the different cases considered, at different locations from the bed, a quadrant analysis of the streamwise and bed-normal velocity fluctuations is performed to obtain a statistical picture of the Reynolds stress distribution. The probability $P(\xi) = Pr\{\tilde{u}'\tilde{w}' = \xi\}$ that the local instantaneous Reynolds stress takes a value ξ is computed from the $\tilde{u}' - \tilde{w}'$ scatter plot. Traditionally the $\tilde{u}' - \tilde{w}'$ scatter plot is divided into four quadrants, of which the second and fourth quadrants (Q2 and Q4) contribute to negative Reynolds stress and have been recognized to be the most significant. A Q2 event corresponds to $\tilde{u}' < 0$ and $\tilde{w}' > 0$, while a Q4 event corresponds to $\tilde{u}' > 0$ and $\tilde{w}' < 0$. A Q4 event will bring the higher-momentum fluid from the bulk flow close to the bed, while a Q2 event will cause low-momentum fluid present close to the bed to be ejected into the bulk flow. Vertical mixing due to Q2 events leads to resuspension of settling sediments. Also, Q2 events correspond to quasi-streamwise and hairpin vortices in the flow which are responsible for sustaining turbulence. Therefore negative Reynolds stress contributions from Q2 and Q4 events are separated when computing the probability.

Figure 13 shows $|\xi P(\xi)|$ versus the Reynolds stress value (ξ) for the second quadrant events at $\tilde{z}^+ = 18$ for cases 0 and 5. Results for other bed-normal locations and for other cases are similar and therefore not shown. The Reynolds stress at which $|\xi P(\xi)|$ reaches a peak value is denoted by ξ_m, which can be interpreted as the turbulent event that makes the largest contribution to the time and horizontally

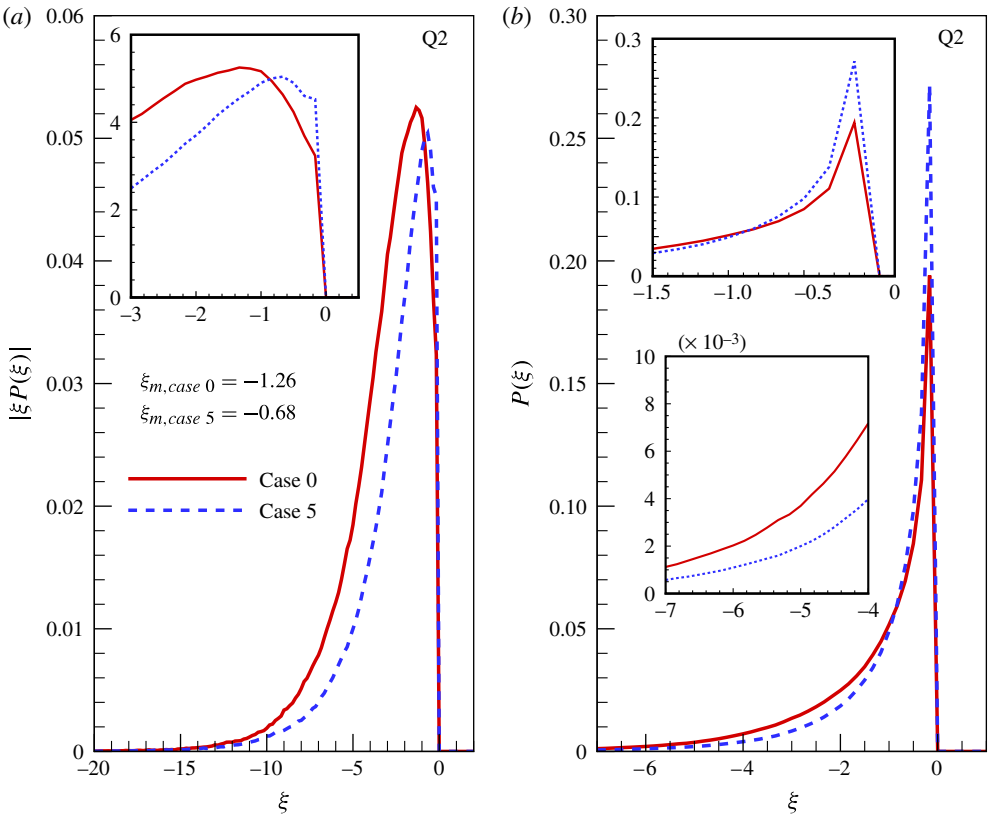

FIGURE 13. (Colour online) (*a*) Weighted probability density function of Q2 events. (*b*) Probability density function of Q2 events. The bed-normal location is $z^+ \sim 18$. ξ_m is the maximizing Reynolds stress Q2 event and its value for cases 0 and 5 is shown in (*a*). The inset in (*a*) highlights the change in the maximizing Reynolds stress Q2 event from cases 0 to 5. The insets in (*b*) show the region around the most probable Q2 event (ξ_p), which does not change from cases 0 to 5, and the bottom part of the curves.

averaged mean Reynolds stress. For case 0, contribution to the mean Reynolds stress is maximized for $\xi_m = -1.26$ and the corresponding value of the turbulent event (fluctuating velocity) is $\tilde{\boldsymbol{u}}'_m = (-2.42, 0.0, 0.521)$. The conditionally averaged flow field (conditional eddy) corresponding to this Reynolds stress event is a hairpin vortex (see Adrian 1994). So the question of turbulence sustainment can be posed in terms of the ability of this Reynolds stress maximizing hairpin vortex to produce and populate the subsequent generations of vortical structures (Adrian 2007). In the clear fluid case (case 0) the turbulent vortical structures are self-sustaining and the turbulence generation continues uninterrupted.

For case 5 the peak contribution to Reynolds stress occurs at a lower value of $\xi_m = -0.68$ and the corresponding turbulent velocity event is $\tilde{\boldsymbol{u}}'_m = (-2.10, 0.0, 0.323)$. As is seen in figure 5(*b*), the mean Reynolds stress for $\tilde{z}^+ = 18$ (peak location) decreases by only $\sim$17 % from cases 0 to 5. However, the strength of the Reynolds stress maximizing event ξ_m has decreased to $\sim$46 %. More importantly, this decrease in Reynolds stress comes about by a 38 % reduction in the bed-normal velocity fluctuations.

Instead of $|\xi P(\xi)|$ one can also look at the Reynolds stress in the second quadrant that maximizes $P(\xi)$. Such an event can be denoted by ξ_p and interpreted as the most likely Reynolds stress event (as opposed to one that maximizes the contribution to the mean Reynolds stress). The most likely Reynolds stress event computed in this manner for case 0 is given by $\xi_p = -0.167$, $\tilde{\boldsymbol{u}}'_p = (-0.505, 0.00, 0.331)$. The corresponding values for case 5 are $\xi_p = -0.167$, $\tilde{\boldsymbol{u}}'_p = (-0.728, 0.00, 0.229)$. The most likely Reynolds stress event does not change with settling velocity, but the turbulent velocity vector changes. From cases 0 to 5 there is 44 % increase in streamwise velocity fluctuations, and a decrease of 33 % in the bed-normal velocity fluctuations. Thus, increase in settling velocity of sediments results in reorientation of the most likely Q2 Reynolds stress event vector while keeping the intensity of the event constant.

Zhou *et al.* (1999) considered conditionally averaged vortical structures in unstratified channel flow obtained for different levels of turbulent Reynolds stress events given by $\alpha^2\xi_m$. As the constant α varied from 0.25 to 3.0, the intensity of the initial vortical structure increased. They observed that only for α greater than 2.0 was the conditional vortical structure able to auto-generate future generations of hairpin and quasi-longitudinal vortex structures. Initial vortical structures of strength α less than 2.0 were unable to auto-generate new vortical structures. From figure 13(*b*) the probability of Reynolds stress events of strength at least four times ξ_m can be computed as $P(\xi < -5.04)$. For case 0 this probability is 4 % at $z^+ \approx 18$ and it is sufficient to spawn the next generation of vortical structures and maintain turbulence in the flow. For case 5 the probability $P(\xi < -5.04)$ has decreased to 2 %. Note that although ξ_m for case 5 is lower than ξ_m for case 0, here the threshold Reynolds stress for regeneration is maintained at 5.04.

It is important to mention that the auto-generation criterion given by Zhou *et al.* (1999) was for unstratified single-phase channel flow and hence cannot be directly extended to stratified multiphase flows. As discussed above, the effect of increased settling velocity of sediments is not only to decrease ξ_m, but also to reorient the event vector $\tilde{\boldsymbol{u}}'_m$ to be increasingly parallel to the bed. As the event vector flattens it is probable that even higher initial vortex strength will be required to spawn the next generation of structures. Thus the value of α is likely to be different and much greater than 2 for auto-generation in the case of flows with suspended sediments. The results of Zhou *et al.* (1999) illustrate the dependence of the threshold amplitude (for regeneration of vortical structures) on the character of the event and thereby on the initial vortex structure. It can therefore be conjectured that when the settling velocity of sediments is increased above the threshold, the change in the spatial structure of the vortical structures combined with the reduction in their strength precludes sustained regeneration of turbulent vortical structures, and ultimately the flow loses all turbulence. Time-resolved movies (to be discussed in § 4.7), which show turbulent vortical structures existing in case 5 and how these structures evolve in case 6, support this viewpoint.

4.7. *Near-bed coherent structures and concentration fluctuations*

With increasing $\tilde{V}$ the settling flux of sediments increases. For the stationary state the settling flux must be balanced by the combination of upward diffusive flux and turbulent flux (mixing) of sediments. In a turbulent flow the diffusive flux dominates only in the region close to the bed. Thus, away from this region, an increase in settling flux demands a concomitant increase in the turbulent flux $\overline{\tilde{w}'\tilde{c}'}$. From figure 6(*b*) it

is evident that the level of vertical velocity fluctuations in fact decrease with $\tilde{V}$, and thus an increase in the turbulent flux of sediments requires a strong increase in the fluctuations of sediment concentration and its correlation with the velocity fluctuations.

Figure 4 shows the variation in both the mean concentration ($\tilde{\bar{c}}_b$) and r.m.s. concentration fluctuations ($\tilde{c}_{rms,b}$) at the bed with increasing settling velocity of sediments. As expected, the mean concentration at the bed gradually increases with increase in settling velocity; however, the r.m.s. concentration fluctuations explosively increase as the critical settling velocity is approached. The r.m.s. value increases by a factor of 5 as the settling velocity of sediments increases from 0.01 to 0.026. For case 1 ($\tilde{V} = 0.01$) the r.m.s. value is $\sim$3 % of the mean concentration, and it increases to 12.5 % for case 5 ($\tilde{V} = 0.026$). The explosive growth in concentration fluctuations indicates local segregation of sediments into regions of much higher concentration than the mean and other regions of much lower concentration than the mean. Furthermore, in order to maintain the stationary state by increasing the turbulent upward flux of sediments, the regions of high concentration must be correlated with regions of upward (positive) bed-normal velocity fluctuation. The existence of such regions of large sediment concentrations would require the flow to locally expend a large amount of energy in order to achieve the required upward bed-normal transport. This can lead to an abrupt shutdown of the auto-generation mechanism of hairpin vortex structures in the flow, which causes a complete collapse of the flow turbulence.

Figures 14 and 15 show plots of streamwise velocity ($\tilde{u}'$), bed-normal velocity ($\tilde{w}'$) and concentration ($\tilde{c}'$) fluctuations for cases 1 and 5 in the $\tilde{x}$–$\tilde{y}$ (streamwise–spanwise) plane at $z^+ \sim 12$. This location $z^+ \sim 12$ is around the region where maximum turbulent kinetic energy production and maximum Reynolds stress are seen. The plots of concentration and streamwise velocity fluctuations show long streamwise aligned streaky structures in both cases. It can be observed that $\tilde{u}'$ and $\tilde{c}'$ distributions are negatively correlated. In other words, the sediment concentration is higher (lower) along the low-speed (high-speed) streaks. The bed-normal velocity fluctuations are also well correlated with the streamwise velocity and concentration fluctuations. But since $\tilde{w}'$ does not show a long streaky structure, the correlation is not as obvious.

From cases 1 to 5 there is a slight reduction in the minimum and maximum values of $\tilde{u}'$ and $\tilde{w}'$, while there is substantial increase in the minimum and maximum values of $\tilde{c}'$. Comparison of the two cases reveals certain interesting features. In the contour plots of case 1, the low- and high-speed steaks and the region of large bed-normal velocity fluctuations, which are indicative of local quasi-streamwise and hairpin vortical structures, are more densely populated and are distributed more or less uniformly over the horizontal plane. With increase in settling velocity the density of low- and high-speed streaks is reduced, and as a result the uniformity of their spatial distribution appears to be lost. In the concentration contours, in case 1 the regions of positive large values are long and thin and spread over the entire plane, while in case 5 these regions are long, thick and more intense, and they are now spatially localized. This suggests a reduction in the density of turbulent vortical structures.

Figures 16–18 show iso-surfaces of swirling strength for cases 0, 5 and 6. Swirling strength is defined as the imaginary part of the complex eigenvalues of the local velocity gradient tensor and has been shown to be very effective in extracting vortical regions in turbulent flows (Zhou *et al.* 1999; Chakraborty, Balachandar & Adrian 2005). These figures present the vortical structures of the turbulent flow at a selected time instant. In cases 0 and 5, the flow remains turbulent, and thus the turbulent structures seen in figures 16 and 17 are representative of what is seen at other times as

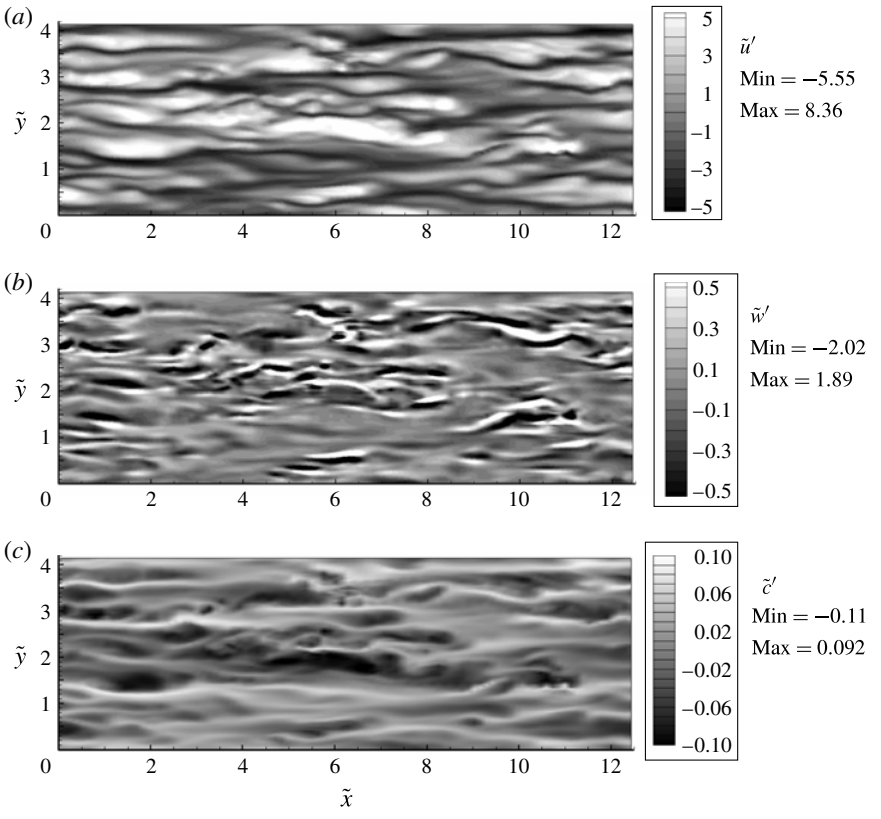

FIGURE 14. (*a*) Streamwise velocity fluctuations. (*b*) Bed-normal velocity fluctuations. (*c*) Fluctuations in the concentration of sediments. Results for case 1 at $z^+ \sim 12$ from the bed.

well. Case 0 shows a dense distribution of hairpin-like and inclined quasi-streamwise vortices in the flow. With increasing settling velocity, the stratification of the flow increases and the structures become sparse, creating pockets in the flow completely devoid of vortical structures. Case 5 corresponds to the closest turbulent case to the critical settling velocity. In figure 17 a substantial decrease in the density of the structures is seen but the flow remains turbulent. This implies that some of the existing structures in the flow are intense enough to spawn the next generation of structures to sustain turbulence. Case 6 corresponds to a settling velocity slightly greater than that in case 5 (∼2 %) and above criticality. At this settling velocity complete turbulence suppression is observed. Figure 18 shows the turbulent structures in case 6 at an instant when the flow is still in the process of turbulence suppression. Note that case 6 was started with a turbulent initial condition taken from case 5 and thus started with vortical structures similar to those shown in figure 17. However, due to the increased settling velocity the auto-generation process was disrupted, and a short time later, as shown in figure 18, the flow has lost most of its turbulent structures. When continued, even the vortical structures seen in figure 18 were not able to spawn the next generation of vortical structures and the flow lost all its turbulent fluctuations (see the λ_{ci} movie for case 6 in the online material available at journals.cambridge.org/flm).

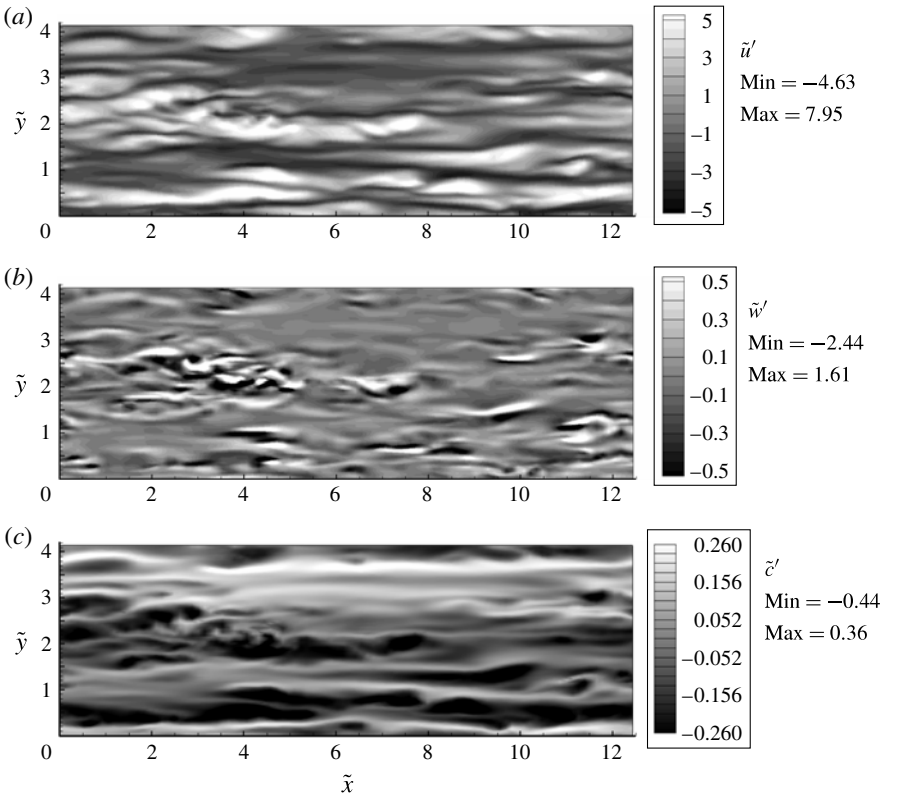

FIGURE 15. (*a*) Streamwise velocity fluctuations. (*b*) Bed-normal velocity fluctuations. (*c*) Fluctuations in the concentration of sediments. Results for case 5 at $z^+ \sim 12$ from the bed.

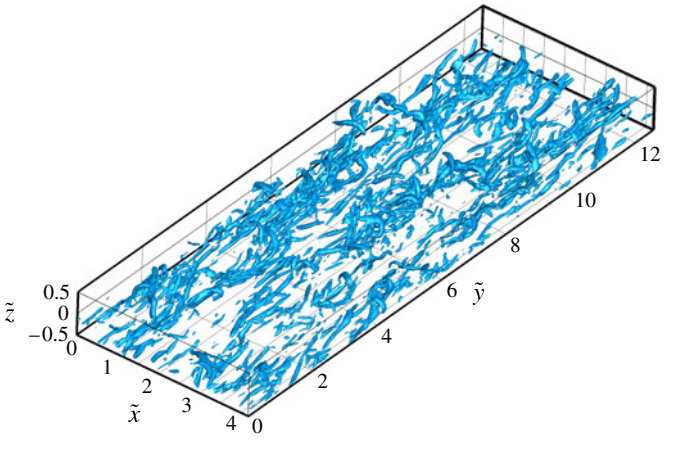

FIGURE 16. (Colour online) Iso-surfaces of λ_{ci} for case 0. The iso-surfaces are $\lambda_{ci} = 22$.

4.8. *Mechanistic view of turbulence suppression*

From the turbulence statistics and the picture of instantaneous turbulent structures presented in the previous sections, the following simple scenario is proposed, which

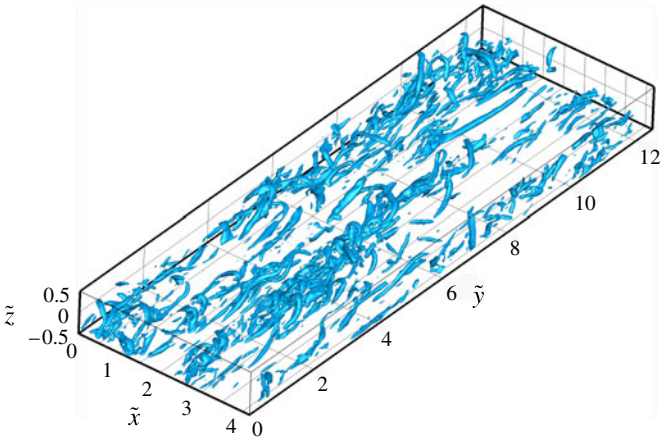

FIGURE 17. (Colour online) Iso-surfaces of λ_{ci} for case 5. The iso-surfaces are $\lambda_{ci} = 22$.

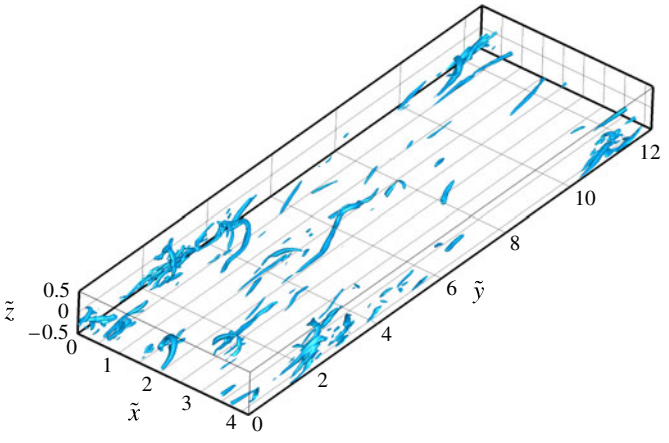

FIGURE 18. (Colour online) Iso-surfaces of λ_{ci} for case 6. The iso-surfaces are $\lambda_{ci} = 22$.

leads to seemingly sudden and abrupt loss of turbulence. For the case of clear fluid auto-generation and turbulence sustainment the mechanisms are well understood. In this limit of zero settling velocity, the sediments are perfectly well mixed at all times with zero concentration fluctuations. As discussed in Zhou *et al.* (1999) the turbulent wall layer is populated with streamwise aligned hairpin vortex packets, and as these packets travel downstream, between their quasi-streamwise legs they cooperatively pump the near-bed low-momentum fluid into the flow. The consequence of this cooperative action of the hairpin packets is the low-speed streaks, which are much longer than the individual hairpin vortices. These streaks provide the environment for subsequent formation of the next generation of hairpin packets.

Consider suddenly introducing a settling velocity for the sediments (this is similar to starting a simulation of non-zero $\tilde{V}$ with case 0 as the initial velocity field). Now sediments are resuspended only in regions of sufficient upward (positive) bed-normal velocity fluctuations, while they settle down in regions of downward fluid motion. This creates increased concentration fluctuations. In particular, the cooperative upward

pumping of fluid by the streamwise aligned hairpin vortex packets provides the perfect environment for the upward transport of sediments. It is in these regions where increased sediment concentrations are expected. Thus, as the hairpin packets travel downstream, similar to the long streaks of low-speed fluid, they leave behind well-correlated long streaks of high sediment concentration. Thus, subsequent generations of hairpin vortices are being formed in regions of steadily increasing sediment concentration.

As seen in the quadrant analysis of the velocity fluctuations, the increased concentration of sediment at the low-speed streaks alters the character of the newly formed vortical structures. Furthermore, the additional buoyancy effect posed by the sediments can be expected to increase the threshold amplitude for the formation of the next generation of vortical structures. Thus, increasing settling velocity of sediments leads to a decrease in the density of vortical structures, whose effect can also be seen in the reduction of the key turbulence statistics. It can then be conjectured that once a threshold settling velocity is exceeded, the local accumulation of sediments at the low-speed streaks do not permit further generation of vortical structures. Without the auto-generation process active, the turbulence over time fully decays.

5. Conclusions

Dilute turbidity currents driven by monodisperse suspension of sediments in bypass mode are modelled as an inclined channel flow driven by suspended sediments. The suspended sediments under the influence of gravity drive the flow in the channel and simultaneously settle towards the bed. The interaction of sediments and turbulence lead to (i) skewing of the streamwise driving force towards the bed, and (ii) stable stratification that damps bed-normal momentum and mass transport. Several simulations of this model were carried out to understand the two effects and their role in turbulence suppression. Simulations S1 and S2 consider flows where the stratification effect in the bed-normal momentum equation is turned off. From these results it is shown that stratification is the dominant effect that brings about total turbulence suppression. Skewing the driving force towards the bed causes turbulence damping but this effect is modest and, even for very large settling velocity, without the stratification effect in the bed-normal momentum equation the flow remains turbulent.

Stratification is the manifestation of the balance between turbulent mixing and the settling of the sediments. At the critical settling velocity, flow turbulence is no longer able to keep the sediments in suspension, and the flow in the channel tends towards the laminar solution. For the present simulations, with $Re_\tau = 180$ and $\theta = 5^\circ$, the mean velocity and mean concentration profiles clearly show that there is sudden transition in the nature of the flow from case 5 ($\tilde{V} = 0.026$) to case 6 ($\tilde{V} = 0.0265$), and thus the critical settling velocity for total turbulence suppression is in the range $(0.026, 0.0265)$. The flow can then be divided into two regimes, i.e. turbulence-stratified flows and turbulence-suppressed flows, and the latter is realized for settling velocities larger than the critical settling velocity. This sudden transition is fascinating, and the abrupt change is seen in several turbulence statistics. This process is similar to the onset of instability, but the difference is its highly nonlinear behaviour. Analysis of the turbulent kinetic energy equation, Reynolds stress transport equation and one-dimensional spanwise and streamwise energy spectra suggest that total turbulence suppression may be brought about by damping of Reynolds stress producing turbulent vortical structures close to the bed.

The term $1/\tan\theta$ in the governing equation can be identified as the Richardson number Ri_τ, which is the ratio of potential energy due to buoyancy effect to kinetic energy of the flow. In the present problem the stratification effect due to sediments is quantified by $R\bar{c}^{(v)}g_zH$, while the kinetic energy of the current can be expressed as $u_*^2 = R\bar{c}^{(v)}g_xH$. Thus, their ratio yields $Ri_\tau = g_z/g_x = 1/\tan\theta$. In an externally driven flow only the buoyancy effect depends on mean sediment concentration, and thus Ri will be a proxy for $\bar{c}^{(v)}$. However, in the present case the flow is driven by the suspended sediments, and as a result $\bar{c}^{(v)}$ appears in both the numerator and the denominator, and Richardson number Ri_τ is simply related to the bed slope. The entire damping process can be represented by the parametric combination of slope of the channel (θ) and settling velocity of the sediments ($\tilde{V}_z$) and the combination takes the form $\tilde{V}_z/\tan\theta$ ($Ri_\tau\tilde{V}_z$) (Cantero *et al.* 2012*b*).

In the work of Zhou *et al.* (1999), it was established that turbulence in an unstratified channel flow sustains itself by auto-generation of vortical structures. They showed that only hairpin vortical structures whose strength is greater than a threshold value are capable of spawning the next generation of structures. The present work proposes an explanation for the abrupt extinction of turbulence in the problem studied using statistical analysis of the Q2 Reynolds stress events for different cases and using the auto-generation criterion given by Zhou *et al.* (1999). From the probability density of these Q2 events it is shown that with increasing settling velocity the intensity of Q2 events decrease and the event vector flattens. These two effects cause spatial modulations in the turbulent hairpin vortices: their intensity reduces and their spatial distribution becomes sparse. As the settling velocity increases beyond the critical value, the threshold vortical strength becomes larger and the existing flow structures are incapable of auto-generating. The flow thus evolves to complete suppression of turbulence.

Acknowledgements

The authors would like to thank the US National Science Foundation for direct and indirect support through the grants OCE 1131016 and OISE 0968313, respectively. The authors would also like to acknowledge the referees for their constructive suggestions which helped improve the quality of this work.

Supplementary movies

Supplementary movies are available at journals.cambridge.org/flm.

REFERENCES

ADRIAN, R. J. 1994 Stochastic estimation of conditional structure: a review. *Appl. Sci. Res.* **53**, 291–303.

ADRIAN, R. J. 2007 Hairpin vortex organization in wall turbulence. *Phys. Fluids* **19** (4), 041301.

ALLEN, J. R. L. 2001 *Principles of Physical Sedimentology*. Blackburn.

BERNARD, P. S., THOMAS, J. M. & HANDLER, R. A. 1993 Vortex dynamics and production of Reynolds stress. *J. Fluid Mech.* **253**, 385–419.

BROOKE, J. W. & HANRATTY, T. J. 1993 Origin of turbulence-producing eddies in a channel flow. *Phys. Fluids* **5**, 1011–1022.

CANTERO, M. I., BALACHANDAR, S., CANTELLI, A., PIRMEZ, C. & PARKER, G. 2009*a* Turbidity current with a roof: direct numerical simulation of self-stratified turbulent channel flow driven by suspended sediment. *J. Geophys. Res.* **114**, C03008.

CANTERO, M. I., BALACHANDAR, S. & GARCÍA, M. H. 2008*a* An Eulerian–Eulerian model for gravity currents driven by inertial particles. *Intl J. Multiphase Flow* **34**, 484–501.

CANTERO, M. I., BALACHANDAR, S., GARCÍA, M. H. & BOCK, D. 2008*b* Turbulent structures in planar gravity currents and their influence of the flow dynamics. *J. Geophys. Res.* **113**, C08018.

CANTERO, M. I., BALACHANDAR, S. & PARKER, G. 2009*b* Direct numerical simulation of stratification effects in a sediment-laden turbulent channel flow. *J. Turbul.* **10**, 1–28.

CANTERO, M. I., CANTELLI, A., PIRMEZ, C., BALACHANDAR, S., MOHRIG, D., HICKSON, T. A., YEH, T., NARUSE, H. & PARKER, G. 2012*a* Emplacement of massive turbidities linked to extinction of turbulence in turbidity currents. *Nature Geosci.* **5** (1), 42–45.

CANTERO, M. I., GARCÍA, M. H. & BALACHANDAR, S. 2008*c* Effect of particle inertia on the dynamics of depositional particulate density currents. *Comput. Geosci.* **34**, 1307–1318.

CANTERO, M. I., SHRINGARPURE, M. & BALACHANDAR, S. 2012*b* Towards a universal criteria for turbulence suppression in dilute turbidity currents with non-cohesive sediments. *Geophys. Res. Lett.* **39** (14).

CANUTO, C., HUSSAINI, M., QUARTERONI, A. & ZANG, T. 1988 *Spectral Methods in Fluid Dynamics*. Springer.

CHAKRABORTY, P., BALACHANDAR, S. & ADRIAN, R. J. 2005 On the relationships between local vortex identification schemes. *J. Fluid Mech.* **535**, 189–214.

CORTESE, T. A. & BALACHANDAR, S. 1995 High performance spectral simulation of turbulent flows in massively parallel machines with distributed memory. *Intl J. High Performance Comput. Appl.* **9**, 187–204.

FERRY, J. & BALACHANDAR, S. 2001 A fast Eulerian method for disperse two-phase flow. *Intl J. Multiphase Flow* **27**, 1199–1226.

GARCIA, M. H. & PARKER, G. 1993 Experiments on the entrainment of sediment into suspension by a dense bottom current. *J. Geophys. Res.* **98**, 4793–4807.

GEYER, W. 1993 The importance of suppression of turbulence by stratification on the estuarine turbidity maximum. *Estuar. Coast.* **16**, 113–125.

HOPFINGER, E. J. 1983 Snow avalanche motion and related phenomena. *Annu. Rev. Fluid Mech.* **15**, 47–76.

KIM, J., MOIN, P. & MOSER, R. 1987 Turbulence statistics in fully developed channel flow at low Reynolds number. *J. Fluid Mech.* **177**, 133–166.

KNELLER, B. C. & BUCKEE, C. 2000 The structure and fluid mechanics of turbidity currents: a review of some recent studies and their geological implications. *Sedimentology* **47**, 62–94.

KRAUSE, D. C., WHITE, W. C., PIPER, D. J. W. & HEEZEN, B. C. 1970 Turbidity currents and cable breaks in the western New Britain trench. *Geol. Soc. Am. Bull.* **81**, 2153–2160.

MUCHA, P. J. & BRENNER, M. P. 2003 Diffusivities and front propagation in sedimentation. *Phys. Fluids* **15** (5), 1305–1313.

NECKER, F., HARTEL, C., KLEISER, L. & MEIBURG, E. 2005 Mixing and dissipation in particle-driven gravity currents. *J. Fluid Mech.* **545**, 339–372.

PARKER, G. 1982 Conditions for the ignition of catastrophically erosive turbidity currents. *Mar. Geol.* **46**, 307–327.

PARKER, G. 2008 Transport of gravel and sediment mixtures. In *Sedimentation Engineering: Processes, Measurements, Modeling and Practice* (ed. M. H. Garcia), pp. 165–252. ASCE.

PARKER, G., FUKUSHIMA, Y. & PANTIN, H. M. 1986 Self-accelerating turbidity currents. *J. Fluid Mech.* **171**, 145–181.

PINET, P. R. 2006 *Invitation to Oceanography*, 4th edn. Jones and Bartlett.

PIRMEZ, C. & IMRAN, J. 2003 Reconstruction of turbidity currents in Amazon channel. *Mar. Petrol. Geol.* **20**, 823–849.

SEGRE, P. N., LIU, F., UMBANHOWAR, P. & WEITZ, D. A. 2001 An effective gravitational temperature for sedimentation. *Nature* **409**, 594–597.

SEQUEIROS, O. E., NARUSE, H., ENDO, N., GARCÍA, M. H. & PARKER, G. 2009 Experimental study on self-accelerating turbidity currents. *J. Geophys. Res.* **114**, C05025.

TALLING, P. J., WYNN, R. B., MASSON, D. G., FRENZ, M., CRONIN, B. T., SCHIEBEL, R., AKHMETZHANOV, A. M., DALLMEIER-TIESSEN, S., BENETTI, S., WEAVER, P. P. E., GEORGIOPOULOU, A., ZUHLSDORFF, C. & AMY, L. A. 2007 Onset of submarine debris flow deposition far from original giant landslide. *Nature* **450**, 541–544.

ZHOU, J, ADRIAN, R. J. & BALACHANDAR, S. 1996 Autogeneration of near-wall vortical structures in channel flow. *Phys. Fluids* **8**, 288–290.

ZHOU, J., ADRIAN, R. J., BALACHANDAR, S. & KENDALL, T. M. 1999 Mechanisms for generating coherent packets of hairpin vortices in channel flow. *J. Fluid Mech.* **387**, 353–396.